1-1-2015

Measurement of Particulate Transition Metals and Atmospheric Processing of Iron

Benton T. Cartledge
University of Denver

Follow this and additional works at: https://digitalcommons.du.edu/etd

Part of the Other Chemistry Commons

MEASUREMENT OF PARTICULATE TRANSITION METALS AND
ATMOSPHERIC PROCESSING OF IRON

_____

A Dissertation

Presented to

the Faculty of Natural Sciences and Mathematics

University of Denver

_____

In Partial Fulfillment

of the Requirements for the Degree

Doctor of Philosophy

_____

by

Benton T. Cartledge

November 2015

Advisor: Brian J. Majestic

Author: Benton T. Cartledge
Title: MEASUREMENT OF PARTICULATE TRANSITION METALS AND
ATMOSPHERIC PROCESSING OF IRON
Advisor: Brian J. Majestic
Degree Date: November 2015

Abstract

The work presented herein details the measurement of particle-bound metals in environmental samples with specific interests in iron (Fe) in atmospheric particulate matter. Metals were measured in ambient $PM_{2.5}$ to study the effects and contributions of a light rail system on the concentrations of metals in atmospheric particles. Particulate matter samples were collected on board trains, near the tracks, and at an urban background location in Denver, CO. Metals were found to be enriched in particles collected on board the trains more so than at the other locations. Fe speciation was also measured in the soluble fraction of the sample and the results showed the contribution of anthropogenic iron to the collected particles.

Lab-created simulated marine particles were used to study the different variables affecting Fe solubility in atmospheric particulate matter during atmospheric transport. The effects of particle size, mineralogy, exposure to sulfur dioxide, and relative humidity were investigated. Particle size and mineralogy were shown to have the largest effect on iron solubility with particles with smaller aerodynamic diameters containing more soluble Fe. Sulfur was incorporated onto the particles however XANES measurements showed no effect on Fe chemistry or speciation.

Fe, Au, and Ag nanoparticles in aquatic matrices were also investigated as part of a two-fold spICPMS experiment. The first study focused on observing formation of Fe

nanoparticles in seawater. This led to the development of a new way to introduce a

sample to the instrument as well as the second study; identifying a particle pulse in the

presence of dissolved analyte. Using well characterized Au particles, a mathematical

method using the mode and standard deviation of the dataset was developed and

successfully used to distinguish a particle signal pulse from that of the background. This

method was validated using a nanotechnology-enabled consumer spray containing both

dissolved and particle Ag. This method allows for more universal use of spICPMS.

Acknowledgements

First and foremost thanks to my Ph.D. advisor, Dr. Brian Majestic for his patience wisdom, and guidance. The knowledge I have gained from my time working with him is invaluable and has made me a better scientist.

Special thanks to my Ph.D. defense committee: Dr. Bryan Cowen, Dr. Alex Huffman, Dr. Keith Miller, and Dr. David Patterson.

Thanks to our collaborators at Arizona State University: Dr. Pierre Herckes, Dr. Ariel Anbar, and especially Dr. Aurelie Marcotte. I owe Aurelie a great deal of thanks for the pain staking preparation of samples.

Thanks to Dr. Gary Bishop at the University of Denver, Dr. Robert Field and Mr. Gary Zito at the Colorado School of Mines, Josep Roque-Rosell at the Lawrence Berkeley National Lab, Pam Skaar at the Wisconsin State Laboratory of Hygiene, and Bradley Rink with CDPHE for assistance with various aspects of this work.

Special thanks to the undergraduates Kyra Whitworth, Matt Iritani, Mariel Price, Eva Cutler, and Allie Phocas for all of your hard work and friendship over the years.

Thanks to Glenn Capodagli, Cole Cronk, Nitika Dewan, Molly Haugen, John Haynes, Randall Mazzarino, Michelle Racey, and Zhelin Yu for their friendship which helped make life all the better.

Thanks to my family for their constant support on this adventure.

Thanks to the love of my life, Lauren, for everything.

iv

Table of Contents

List of Figures

List of Abbreviations and Common Terms

CDPHE: Colorado Department of Public Health and the Environment

EDS: energy dispersive x-ray spectroscopy

EF: enrichment factor

eV: electron volts

EXAFS: extended x-ray absorption fine structure

ICP-MS: inductively coupled plasma mass spectrometry

NP: nanoparticle

PCIS: Sioutas personal cascade impactor sampler

PM: particulate matter

$PM_{2.5}$: particulate matter with aerodynamic diameter less than 2.5 µm

PM_{10}: particulate matter with aerodynamic diameter less than 10 µm

RH: relative humidity

ROS: reactive oxygen species

RTD: Regional Transportation District

SEM: scanning electron microscopy

spICPMS: single particle inductively coupled plasma mass spectrometry

TDS: total dissolved solids

TEM: transmission electron microscopy

UCC: upper continental crust

XANES: x-ray absorption near edge structure

Chapter One: Introduction

1.1 Metals in the Environment

Metals are a large chemical constituent of environmental matrices: soil, water, and air. Metals in the environment are predominantly transported in the particle phase as either atmospheric particulate matter (PM) or suspended particles or nanoparticles in aquatic systems as well as dissolved soluble metals. This is due to metals being abundant in crustal soils and minerals as well as an accumulation into small diameter particles from industrial combustion (Mason 2013). There are both natural and anthropogenic sources of metals to environment with natural sources being the larger contributor.

1.2 Sources of Metals

The crust is by far the biggest natural source of metals to the environment, as it contains nearly 30% of the Earth's budget of these crustal and rare earth elements (Taylor and Mclennan 1995). These natural sources include the physical and chemical weathering of rocks and minerals, volcanic eruptions, sea spray, and wildland fires (Rubin 1974; Connell 2005). Of metals in the crust, aluminum (Al) is the most abundant. Iron (Fe) is the fourth most abundant element in the crust, and most common transition metal in both the crust and PM (Johansen et al. 2000a; Connell 2005).

Anthropogenic sources of metals to air and water include mining and agriculture operations, industrial emissions, urban runoff and wastes, and motor vehicle operation. While a number of the metals typically emitted from anthropogenic sources also occur

naturally, they can be significantly enriched as a result of human activity. Elements such as Fe, Cr, Mn, Pb, Zn, Cu, Cd, Ni, Sb, and As have all been shown to be enriched in environmental matrices as a result of anthropogenic sources (Rubin 1974; Thurston and Spengler 1985; Manoli et al. 2002; Connell 2005; Lough et al. 2005; Querol et al. 2007; Mason 2013). A common method for determining the extent to which a metal is of anthropogenic origin or not is to determine the enrichment factor. Using measured ratios of elements in the continental crust and the concentration of the elements in the sample an enrichment factor can be calculated (Taylor and Mclennan 1995).

In atmospheric PM, the size of the particle and metal content can also be an indicator of source. Crustal particles of natural origin are typically larger (aerodynamic diameter >1 µm) and consist of the common crustal elements while anthropogenic particles, especially those resulting from combustion processes, are typically smaller in size (aerodynamic diameter < 1µm) and have elevated concentrations of metals typically associated with anthropogenic sources (Cass and McRae 1983; Lighty et al. 2000; Singh et al. 2002; Song et al. 2006). This is important as smaller particles can be transported further leading to longer transport of anthropogenic metals. Also, smaller particles can bypass the natural defenses of the body and penetrate deeper into the lungs leading to increased toxicity of smaller particles.

1.3 Metals in Aquatic Matrices

Once in the air, water, and/or soil, metals participate in a large variety of chemical processes. Metals in the environment can serve as electron acceptors, allowing the participation in a number of chemical reactions. In aquatic systems, the solubility of trace metals is controlled by pH, presence of electron donors and chelating ligands (such

as organic matter), and the oxidation state of the metal and redox environment (Connell 2005; Mason 2013). As a result, metals in aquatic environments are partitioned between the particle and dissolved phases and commonly associated with colloids or metal/metal oxide nanoparticles (Benoit et al. 1994; MacDonald et al. 2000; Turner and Millward 2002). Ultimately, a large quantity of the metals are exported from freshwater systems to the world's oceans (Zhang 1995; Macdonald et al. 2005). This mechanism of transport results in the majority of metals settling out into the sediment in coastal regions and estuaries as a result of changes in pH and ionic strength, salinity, and settling of suspended particles. Metals, such as Fe and Mn, can be released from sediment back into the dissolved phase as a result of chemical and physical transformations. Fe and Mn are much more soluble in reduced forms Fe(II) and Mn(II) (Stumm and Morgan 1996; Majestic et al. 2006; Majestic et al. 2007b) and can be released from sediment through oxidation and reduction cycles especially in low oxygen environments (Chester and Jickells 2012). Studies of remote regions of the oceans known as high-nutrient low chlorophyll (HNLC) where macronutrients (nitrate and phosphate) are in abundance yet chlorophyll levels (a measure of biological growth) are low, suggest the importance of the atmospheric deposition of metals, such as Fe (an important micronutrient for phytoplankton) into these HNLC regions of the oceans (Falkowski et al. 1998; Field et al. 1998; Moore et al. 2002; Jickells et al. 2005; Mahowald et al. 2005; Boyd et al. 2007).

1.4 Metals in the Atmosphere

Atmospheric deposition of PM into the world's oceans occurs through either wet or dry deposition with dry deposition occurring nearer to the source and wet deposition being further (Seinfeld and Pandis 2006). Atmospheric PM can be transported long

distances from the source, often depending on particle size, providing significant amounts

of both crustal and anthropogenic metals to the oceans (Duce et al. 1991; Prospero et al.

2002; Mahowald et al. 2005; Baker and Jickells 2006; Chin et al. 2007; Kallos et al.

2007). This transport of PM to oceans serves as an important supply of micronutrient

metals to microorganisms (Jickells et al. 2005). This also poses another important

question, one that developed the crux of the work presented herein; how do chemical

transformations during atmospheric transport of these metals affect the solubility

(especially Fe) in seawater and, thus, the overall bioavailability? For instance, Fe is only

marginally soluble in seawater (0-2%) leading to an Fe concentration of about 2 nM and

50-60% of that fraction being colloidal (Wu et al. 2001; Bergquist et al. 2007; Baker and

Croot 2010; Sholkovitz et al. 2012). At the same time however, measurements made of

Fe in PM collected over remote regions of the ocean observed Fe solubility as high as

50% (Zhuang et al. 1992; Sholkovitz et al. 2009; Sholkovitz et al. 2012). All of these

discrepancies in the measurements were a major driving force behind the works presented

in Chapters 3 and 4.

1.5 Health Effects of Metals

Another significant motivation behind the work presented herein are the adverse

health effects linked to the inhalation of metal-containing PM. The effects of the

inhalation of PM has been a well-studied topic and a major motive for the study of PM.

Studies have shown that the exposure to PM, especially fine PM (aerodynamic diameter

< 2.5 µm) can lead to increases in asthma (or exacerbation of pre-existing asthma), other

respiratory illnesses, and mortality (Dockery et al. 1993; Mortimer et al. 2002; Pope and

Dockery 2006). More recently, studies have linked the formation of reactive oxygen

species (ROS) to negative health effects of PM, as well as lung cancer and cardiovascular diseases (Valavanidis et al. 2005; Hu et al. 2008). A number of studies have also linked the formation of ROS to transition metals in the PM (Goldsmith et al. 1998; Tao et al. 2003; Prophete et al. 2006; Landreman et al. 2008; Verma et al. 2010). Further investigations analyzed personal exposure to metals in PM and a few of those went as far as to correlate particular redox metals such as Fe, Cr, and Ni to ROS activity (Chillrud et al. 2004; Chillrud et al. 2005; Kam et al. 2011b; Kam et al. 2013). Soluble metals in PM have also been shown have a larger correlation to the negative health effects of PM exposure as the metals are more biologically active when in a more soluble state (Ghio et al. 1999; Verma et al. 2010). Due to the prevalence of Fe in ambient PM, and its ability to form ROS via Fenton chemistry, the solubility and speciation or Fe in PM is of particular interest in terms of negative health effects (Halliwell and Gutteridge 1986; Karlsson et al. 2005; Faiola et al. 2011; Kam et al. 2011b). These health effects were a major motive for the work discussed in Chapter 2.

1.6 Measurement Techniques

It has become increasingly important to be able to measure and study metals in particles in the different environmental matrices. The most sensitive method for the trace level quantitation of metals is inductively coupled plasma mass spectrometry (ICP-MS). Other wet-chemical quantitative techniques include atomic absorption spectroscopy (AA), inductively coupled plasma atomic emission spectrometry (ICP-AES), and x-ray fluorescence (XRF). Chemical speciation can also be measured using x-ray absorption near edge structure spectroscopy (XANES), and extended x-ray absorption fine structure (EXAFS). All of these methods are viable options for the measurement of metals in

environmental matrices; however the wet-chemical methods require dissolving or destroying the particle and yield no useful information regarding speciation and molecular coordination.

The speciation of a metal in an environmental sample also allows an understanding of source, bioavailability, and other chemical properties of the metal. Techniques such as XANES and EXAFS have been utilized to study the metals while still in particle form. XANES, used to study Fe speciation in Chapter 3, uses a high energy x-ray to excite a core electron. When a higher energy core electron relaxes to fill the core hole a fluorescent photon is emitted. The energy of the fluorescent photon is characteristic of the atom and electron that fills the hole. For the XANES measurements of Fe presented in Chapter 3, the K-edge absorption peak was used to distinguish between Fe(II) and Fe(III). The K-edge relates to the excitation of a 1s electron. For Fe, the K-edge energy of Fe(II) is approximately 4 eV less than that of Fe(III) likely due to a lower energy valence 3d electron in Fe(II). This is highlighted in Figure 1.1 where the XANES spectra of Fe(II) and Fe(III) oxides are shown.

Several studies have successfully measured metal speciation and composition in various types of samples. Examples of these measurements include Fe and V in ambient PM (Majestic et al. 2007a; Shafer et al. 2012), Fe in automobile exhaust (Oakes et al. 2012a), and Cr, Mn, Fe, Cd, and Zn in soot and industrial activities (Werner et al. 2006; Sammut et al. 2008; Nico et al. 2009; Sammut et al. 2010).

A new and developing technology for the measurement of nanoparticles in aquatic systems is single particle inductively coupled plasma mass spectrometry (spICPMS). Nanoparticles, whether naturally occurring or engineered (ENP),
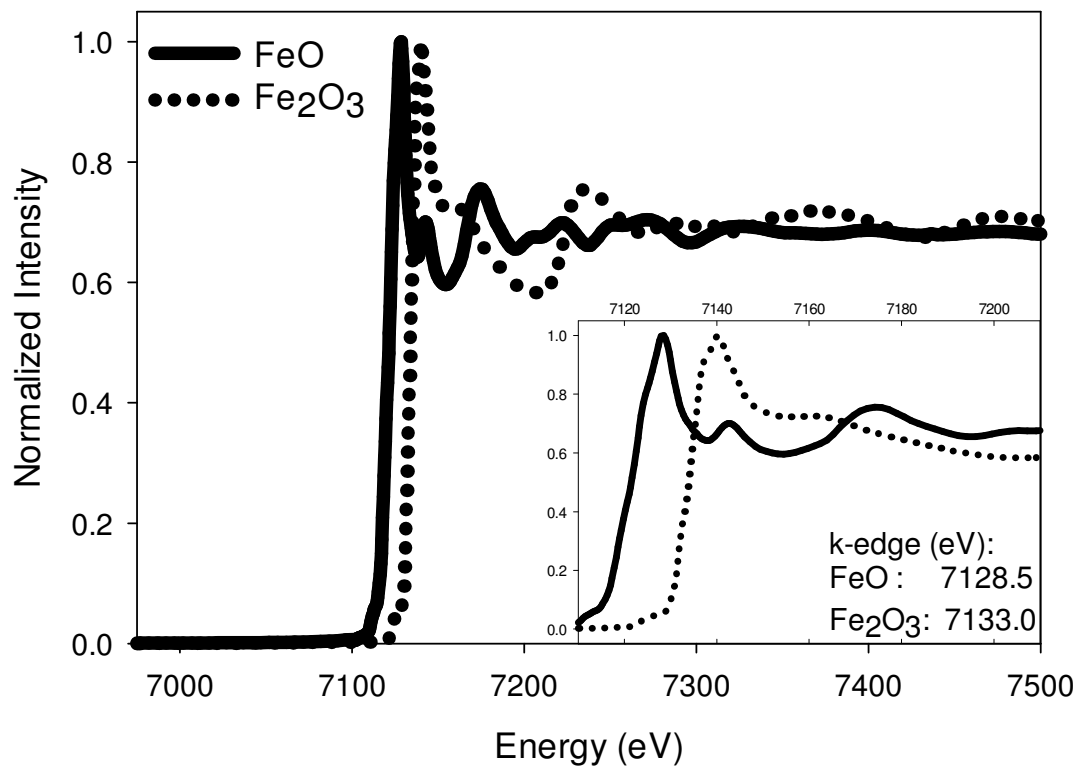
Figure 1.1: XANES spectra of Fe(II) (solid line) and Fe(III) (dotted line) oxides. Inset figure more clearly shows the difference in K-edge energy between the two Fe oxidation states

are a topic of a large volume of recent research (Leitch et al. 2012). Using the principles

of ICP-MS, nanoparticles can be sized and counted in a variety of matrices (Pace et al.

2011; Pace et al. 2012; Montano et al. 2014). This technique is element specific and

offers a quick and high sample volume alternative to traditional particle sizing techniques

such as scanning electron microscopy (SEM) and transmission electron microscopy

(TEM).

1.7 Summary of Subsequent Chapters

Given the prevalence of metals in the environment and the potential

environmental and health related impacts, the work presented in Chapters 2-4 details the

measurement of metals in atmospheric PM and aquatic systems. Chapter 2 starts with a

broad approach measuring the PM concentration and metal content of ambient PM

collected in Denver and PM related to light rail activity. This study helped further the

knowledge of the effects of rail activity on PM-metal concentrations as well as

contributed to the growing knowledge base about PM in the Denver area. Chapter 3

focuses solely on Fe and Fe solubilization through atmospheric transport. In this study,

lab-created samples are used to manipulate and study variables controlling Fe solubility

in PM to further elucidate which of these variables has the greatest affect. Finally,

Chapter 4 highlights the development of a new mathematical approach for the treatment

of spICPMS data in order to distinguish a nanoparticle signal from that of a dissolved

analyte background allowing for a more accurate analysis of environmental samples.

Chapter Two: Metal concentrations and soluble iron speciation in fine particulate

matter from light rail activity in the Denver-Metropolitan area*

2.1 Abstract

Fine particulate matter samples ($PM_{2.5}$) were collected from three locations

around the Denver-Metropolitan area to study the impacts of the ground-level light rail

on airborne metal concentrations. Size-segregated PM was collected on board the trains,

at the side of the tracks, and at a background location in downtown Denver. Results from

this study showed highest crustal enrichment factors of metals in samples collected on

board the train, despite lower concentrations of total $PM_{2.5}$. Metals commonly found in

steel, such as Fe, Cr, Mn, and Ni, all exhibited elevated concentrations relating to train

activity over the background site. Iron in the $PM_{2.5}$ at track-side and on board the trains

was above the background by a factor of 1.89 and 1.54, respectively. For Mn, the ratios

were 1.34 for the track-side and 0.94 for the on board samples. Cr and Ni exhibited

higher ratios over the background only in samples collected on board the trains at 1.59

(Cr) and 1.26 (Ni). Soluble metals were measured with Ni (53-71%), Cu (52-81%), and

Zn (30-81%) exhibiting the highest solubilities across the different sites. Soluble Fe

ranged from 8-15% for the total measured Fe, indicating a non-crustal source of Fe.

Soluble Fe was also characterized as Fe(II) and Fe(III) with 87-90% of the soluble Fe

being Fe(II), similar to results from studies in Los Angeles, CA and East St. Louis, IL but higher than in Atlanta, GA and Waukesha, WI.

2.2 Introduction

Railway based transportation systems are becoming a more widely used method of mass transportation as cities continue to grow and become less centralized. The long-term exposure to PM from subway and light rail transit systems has been of special interest as more of these types of transportation systems are developed. Railway studies in New York City (Chillrud et al. 2003; Chillrud et al. 2005), Los Angeles (Kam et al. 2011a; Kam et al. 2011b; Kam et al. 2013), Barcelona (Querol et al. 2012), Mexico City (Mugica-Alvarez et al. 2012), Helsinki (Aarnio et al. 2005), Tokyo (Furuya et al. 2001), Budapest (Salma et al. 2007), Stockholm (Johansson and Johansson 2003; Karlsson et al. 2005), Hong Kong (Chan et al. 2002), Buenos Aires (Murruni et al. 2009), Seoul (Kim et al. 2008; Kim et al. 2014), Taipei (Cheng and Lin 2010), Paris (Raut et al. 2009), and London (Adams et al. 2001; Seaton et al. 2005) have shown elevated levels of $PM_{2.5}$ as a result of train activities relative to urban ambient conditions. In many cases, increased concentrations over the background of chromium, manganese, iron, nickel, and copper have been observed in PM collected from these systems (Furuya et al. 2001; Chillrud et al. 2003; Aarnio et al. 2005; Chillrud et al. 2005; Salma et al. 2007; Kam et al. 2011b; Mugica-Alvarez et al. 2012; Kam et al. 2013). PM from these rail systems is generated by the frictional processes and wearing between the wheels, rails and brakes. Since rail-based transit systems vary greatly from each other, results from one system do not always apply to another system (Kam et al. 2011b).

Large amounts of research have linked chronic exposure to PM and certain metals to a wide array of diseases and cancers through the formation of reactive oxygen species (ROS) and oxidative stress on the respiratory system (Goldsmith et al. 1998; Tao et al. 2003; Prophete et al. 2006; Landreman et al. 2008; Verma et al. 2010). The studies performed in Los Angeles (Kam et al. 2011b) and Stockholm (Karlsson et al. 2005) have studied the effects of PM samples collected from rail systems on oxidative stress and ROS activity in alveolar macrophage cells. Per unit mass, Kam *et al.* (2011b) showed that ROS activity increased by 13% from the samples collected on the ground-level light rail. However on a per volume of air basis, which was used to represent personal exposure, the subway samples exhibited higher ROS activity by 55-65% (Kam et al. 2011b). The study in Stockholm found that the PM collected from the subway was eight times more genotoxic than other PM and more likely to cause oxidative stress to lung cells (Karlsson et al. 2005). Studies have also shown links to ROS activity from the soluble fraction of PM (Verma et al. 2010) as well as the particle size (Hu et al. 2008).

Iron (Fe) is of particular interest as it is the most abundant transition metal in the atmosphere and the fourth most abundant element in the earth's crust (Johansen et al. 2000b; Jickells et al. 2005). Fe has also been identified as a component of PM that leads to formation of ROS through Fenton chemistry (Goldsmith et al. 1998; Prophete et al. 2006). The study performed in the Stockholm subway showed that the mass of the particle was dominated by Fe and related this finding to the genotoxicity of the subway samples (Karlsson et al. 2005). The redox activity of Fe and the ability of intracellular formation of ROS has also been related to the amount of Fe in the soluble fraction (Kam

11

et al. 2011b) as well as the Fe speciation [soluble Fe(II) or Fe(III)] (Halliwell and Gutteridge 1986; Faiola et al. 2011).

This study focuses on the measurement of metals and soluble Fe speciation in $PM_{2.5}$ (particles with an aerodynamic diameter less than 2.5 µm) across all five lines of the Regional Transportation District (RTD) light rail system in the Denver-Metropolitan area, CO, USA. Due to the complex nature in which PM can affect the respiratory system and the wide array of differences in railway systems, it is important to study transit systems individually; especially in the pretenses of this study as Denver's light rail is completely at ground level and most previous studies have focused on underground systems. Samples were collected on board the trains, track-side, and at a downtown location 0.28 km from the tracks. In all three locations, $PM_{2.5}$ mass, size-fractionated total metals, soluble metals, soluble Fe(II), and soluble Fe(III) are reported. This is the first study to report soluble Fe redox speciation potentially originating from a light rail system. In addition, this was the first study to report soluble Fe speciation in the city of Denver, CO. As mentioned previously, soluble Fe speciation has implications on ROS production in the lungs, and the understanding of Fe speciation in PM is extremely limited in all but a few urban areas around the USA.

2.3 Materials and Methods

2.3.1 Sample Collection Methods

Samples were collected at three locations: first, on board trains running on each line and second, at two stationary sites, one northeast and one southwest of downtown Denver, CO, USA. The track-side stationary site southwest of downtown was located at

ground-level 1 m from the tracks where all five lines entered and exited downtown

Denver. Figure 2.1 shows a map of the relative location of the sample collection sites. At

this site, all trains passing through this area were braking to pass through curves leading

into the downtown area. Also, southbound trains (leaving downtown) were frequently

stopped here to let northbound pass due to the track alignment that forced them to cross

the northbound tracks. On average, 31 trains pass through this area per hour during the

time frame used for sample collection. The site located to the northeast of downtown

Denver was located at a Colorado Department of Public Health and the Environment air

monitoring station, which represents urban ambient conditions. This site is 0.28 km from

the nearest light rail tracks. The samples collected on board the trains were collected on

each of the five train lines every day of the sample collection periods. A sampler was

attached to a backpack and placed in a seat away from the doors. Samples were only

collected while on the train and not on the platform.

At all sites, PM samples were collected three times a week from January 24 to

February 16, 2012 using 5 Sioutas Personal Cascade Impactor Samplers (PCIS, SKC

Inc.) (Misra et al. 2002; Singh et al. 2003). Two samplers were co-located at each

stationary site (downtown and track-side) and one was carried onboard the trains. The

PCIS, operating at 9 L min^{-1} collected size-resolved PM fractions in five different stages:

>2.5, 2.5-1, 1-0.5, 0.5-0.25, and <0.25 μm. However, only the PM$_{2.5}$ fraction, the four

smallest size fractions, was analyzed in this study. Samples at the two stationary sites

were collected for 14 hours a day, while on-train samples were collected simultaneously
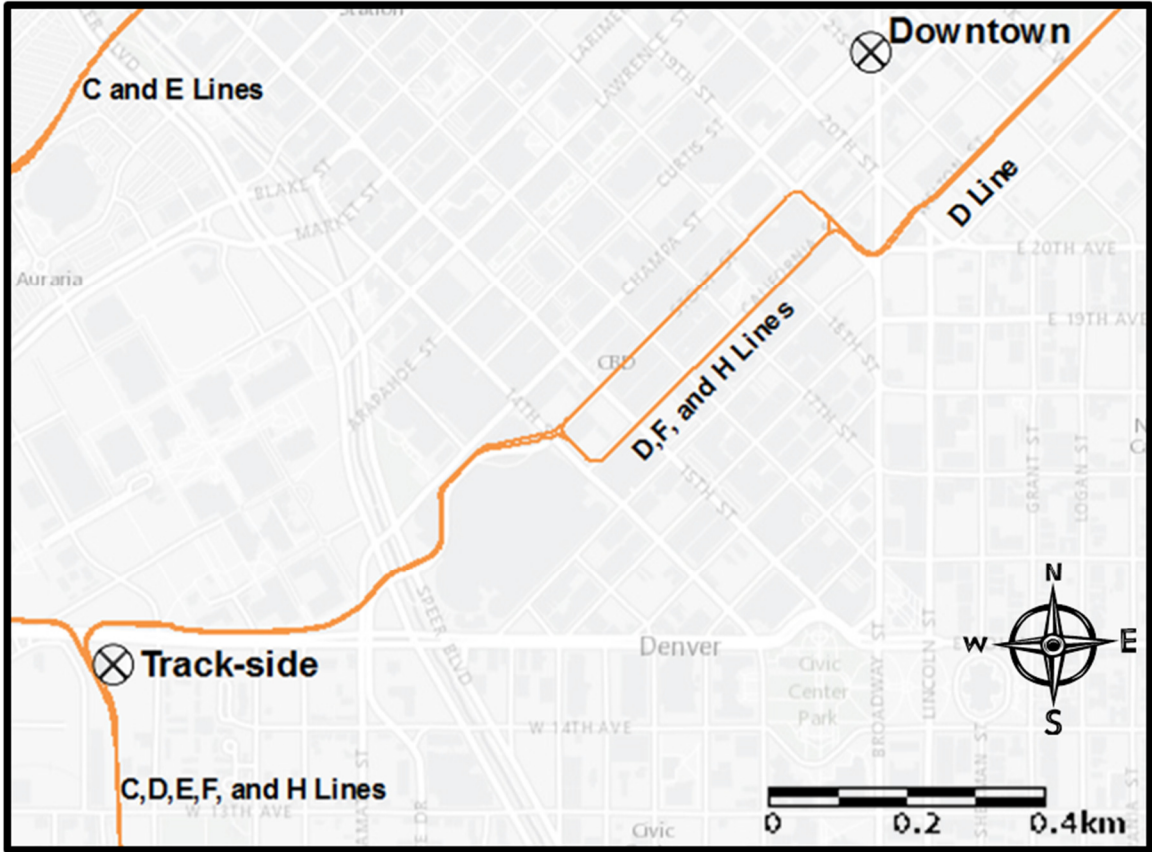
Figure 2.1: Map detailing the relative locations of the sample collection sites

for 12 hours a day. This time scale allowed for the collection of samples before, during, and after both the morning and evening rush hours (6-9 am and 3-7 pm).

Acid-washed Teflon collection substrates for the largest four size fractions were 0.5 μm pore size 25 mm Zefluor (Pall Life Sciences) filters, while 2.0 μm pore size 37 mm Teflo (Pall Life Sciences) filters were used for the smallest size fraction. After each sampling period, substrates were removed, placed into acid-washed Petri dishes, and into a freezer at -18 °C. Field blanks were also collected at each site at the beginning of each sampling period.

2.3.2 Gravimetric Analysis

Prior to and following sample collection, all four sets of filters (112 filters in all) were equilibrated for 24 hours in a constant temperature (23-24 °C) and humidity (31-33%) environment and weighed on a microbalance (MX5, Mettler-Toledo; uncertainty ± 5µg). Field blanks were collected prior to each collection period and measured elemental concentrations were subtracted from the elemental concentrations of the samples. The $PM_{2.5}$ mass was determined by summing the masses of the four smallest size fractions. The gravimetric measurements were compared to an on-site tapered element oscillating microbalance (TEOM) collecting $PM_{2.5}$ mass data every hour at the background location.

2.3.3 Total Metal Analysis

With two sets of samples from each stationary site, one set was used for total metals analysis while the other set was used to assess soluble metal concentrations. The filters for the samples collected on board the trains were cut in half in order to perform both total and soluble metals analyses. Solubilization of the metals was achieved using a

microwave digestion system (Ethos EZ, Milestone, Inc). Samples were digested in a

Teflon vial using 750 μl nitric acid (Fisher), 250 μl hydrochloric acid (Fisher), 100 μl HF

(Fisher), and 100 μL hydrogen peroxide (Fisher). All acids and the hydrogen peroxide

were trace-metal grade purity. Samples were digested in Teflon vessels following a

temperature program of a 9 minute ramp to 180 ℃, a hold at 180 ℃ for 10 minutes, and a

60 minute cool-down period. Following digestion, samples were diluted to 15 mL using

Milli-Q (18.2 MΩ-cm) water and analyzed via quadrupole inductively-coupled plasma

mass spectrometry (ICP-MS, Agilent 7700) using indium as internal standard and a He

collision cell to remove polyatomic interferences. Detection limits via PCIS collection

and ICP-MS analysis have been previously studied and are near 1 ng m^{-3} for most metals

(Majestic et al. 2008).

Standard reference materials (SRMs) were also digested by this same process.

The two SRMs used were Urban Particulate Matter (1648a, NIST), to represent the

anthropogenic portion of the sample, and San Joaquin Soil (2709a, NIST), to represent

the crustal portion of the sample. The acceptable percent recovery of elements from

these SRMs was set at 80-120%. One of each SRM was digested per 21 samples as well

as one method blank which consisted solely of the digestion matrix. Field blanks were

also digested as samples using the method described above.

2.3.4 Soluble Metal Analysis

For soluble metal analysis, the samples were extracted in 10 mL of a 0.5 mM

acetate buffer (pH=4.25), to simulate cloud water, for two hours. The extracts were then

filtered, acidified with HNO$_3$, and analyzed using ICP-MS. The pH of the extract

remained within 4.25 ± 0.01 over the course of the extraction (Accumet Basic AB 15, Fisher Scientific).

2.3.5 Iron Speciation Analysis

Iron speciation analysis was performed using the soluble extracts by mixing 1.8 mL aliquots of extract (prior to acidification) with 0.2 mL of 5.88 µM Ferrozine reagent [(3-(2-pyridyl)-5,6-diphenyl-1,2,4-triazine-4',4"-disulfonic acid sodium salt), Sigma] (Stookey 1970; Majestic et al. 2006). Using a 1 m liquid waveguide capillary cell spectrophotometer (LEDSpec, WPI, Inc.), the absorbance of the Fe(II)-Ferrozine complex was measured at 560 nm. Fe(II) concentration was determined using a calibration curve generated from stock Fe(II) solutions. Fe(III) was then determined by subtraction the Fe(II) concentration from the total Fe concentration obtained from ICP-MS analysis.

2.4 Results

Figure 2.2 shows the size distribution of $PM_{2.5}$ mass at all three sites. $PM_{2.5}$ mass was obtained by summing the four smallest size fractions. The highest $PM_{2.5}$ mass concentrations were measured at the track-side sample site while the lowest mass concentrations were collected on board the trains. The $PM_{2.5}$ concentrations collected at the downtown site were well correlated with the TEOM measurements made by the Colorado Air Monitoring Program (CAMP) at the same site (slope=1.109, R^2= 0.9999) indicating that the samplers were functioning properly (Appendix A). The geometric mean and standard deviation of the different size fractions were similar at all three sampling locations as shown in Appendix A (Hinds 1999).
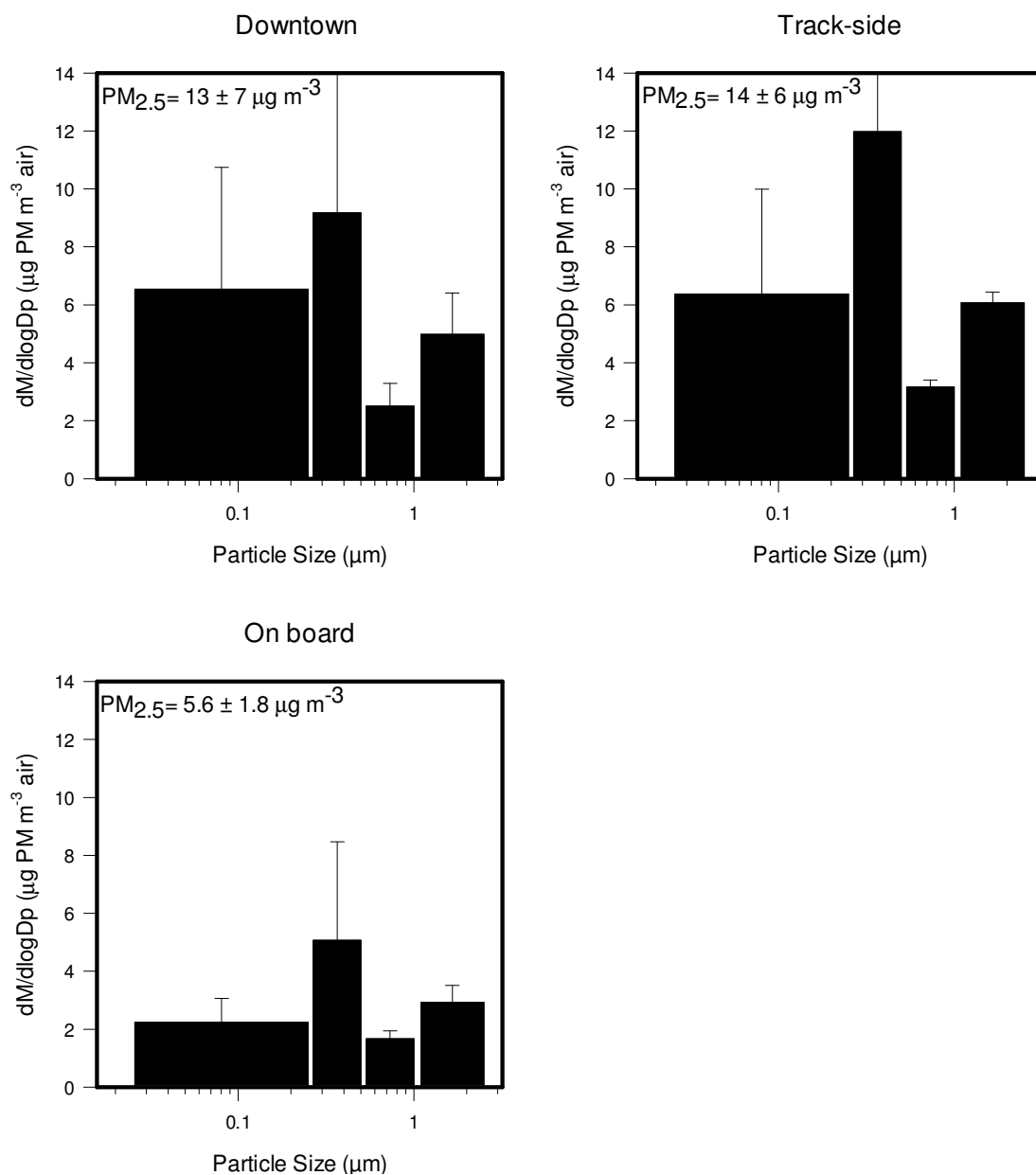
Figure 2.2: Average size-segregated PM$_{2.5}$ concentrations at each sample collection site. Overall PM$_{2.5}$ mass was obtained by summing the PM masses of the four smallest size fractions. The masses of each size fraction were averaged across the three weeks of the campaign and the error bars represent the standard deviation of the PM masses over that time period. The error bars for the second smallest size fraction at the downtown and track-side sites extend to 16 and 20 µg m^{-3} respectively.

Table 2.1 shows elemental concentrations and elemental ratios between sites. Na, Al, K, Ca, Fe, Cu, Zn, Sb, and Pb concentrations were higher than those measured in a recent study in Denver, CO, where $PM_{2.5}$ was collected at two elementary schools in residential neighborhoods (Clements et al. 2014). Of the measured elements in both studies, only As was measured at similar concentrations. In Table 2.1 it can also be seen that on board the train and even more so at track-side, there were higher ratios of Fe over the background site. For Fe, the ratios above the background site are 1.89 and 1.54 for the track-side and on board samples respectively. For Mn, another common element in steel, the ratios are 1.34 for the track-side but only 0.94 for the on board samples. Samples collected on board the trains also showed higher ratios over the background in Cr (1.59), Ni (1.26), and Zn (1.49), which were not as high at the track-side site.

The enrichment of the various metals was measured using the upper continental crust (UCC) enrichment factor (EF) calculated by first normalizing the data with aluminum and then dividing by the UCC ratio (Taylor and Mclennan 1995). The EF shows the extent that anthropogenic sources contribute to the metal concentrations and these are shown in Figure 2.3. The dashed line (EF= 10) on the plot represents the level above which an element is considered to be contributed largely from anthropogenic sources. When the concentration of a particular element is normalized to Al, a predominately crustal element, the EF is calculated based on the naturally-occurring abundance of those elements. A high EF (EF>10) suggests a source of that particular metal that is not naturally occurring and a source that is most likely anthropogenic (Dasch and Wolff 1989; Gerdol et al. 2000; Veysseyre et al. 2001).

Table 2.1. Total elemental concentrations at each site and site-to-site ratio for PM$_{2.5}$.

Site:	Downtown (CAMP)	Track-side (RTD)	On board (LR)		
Element	Conc. (ng m^{-3})	Conc. (ng m^{-3})	Conc. (ng m^{-3})	RTD/CAMP	LR/CAMP
Na	170 ± 110	110 ± 50	180 ± 120	0.65	1.06
Mg	36 ± 16	30 ± 9	33 ± 21	0.83	0.91
Al	180 ± 50	110 ± 30	80 ± 50	0.61	0.44
K	130 ± 80	63 ± 14	180 ± 50	0.49	1.38
Ca	230 ± 140	150 ± 37	450 ± 190	0.65	1.96
Sc	0.16 ± 0.008	0.09 ± 0.01	0.26 ± 0.25	0.54	1.64
Ti	10.98 ± 0.18	9.0 ± 2.6	9.7 ± 2.2	0.82	0.88
V	0.31 ± 0.06	0.27 ± 0.07	0.16 ± 0.06	0.89	0.53
Cr	4 ± 4	2.2 ± 0.5	7 ± 4	0.52	1.59
Mn	6 ± 3	7.6 ± 2.1	5.3 ± 2.6	1.34*	0.94*
Fe	190 ± 50	360 ± 80	292 ± 130	1.89*	1.54*
Co	0.10 ± 0.03	0.10 ± 0.02	0.16 ± 0.10	1.03	1.56*
Ni	1.8 ± 1.3	1.12 ± 0.07	2.2 ± 1.7	0.63	1.26*
Cu	90 ± 70	30 ± 3	41 ± 16	0.33	0.46
Zn	38 ± 23	30 ± 5	57 ± 25	0.79	1.49
As	0.20 ± 0.17	0.19 ± 0.10	0.15 ± 0.08	0.97	0.72
Rb	0.23 ± 0.10	0.19 ± 0.06	0.17 ± 0.04	0.85	0.72
Sr	1.2 ± 0.5	1.5 ± 0.4	1.4 ± 1.0	1.25	1.18
Mo	0.08 ± 0.03	0.09 ± 0.03	0.11 ± 0.04	1.07	1.34
Cd	0.9 ± 0.5	0.65 ± 0.15	1.3 ± 0.7	0.68	1.36
Sn	27 ± 18	17.1 ± 2.6	23 ± 13	0.63	0.85
Sb	1.4 ± 0.4	1.39 ± 0.23	1.7 ± 0.6	0.96	1.17
Ba	9 ± 3	15.1 ± 1.9	11.8 ± 2.9	1.67	1.30
Pb	2.1 ± 0.4	1.58 ± 0.20	1.4 ± 0.4	0.75	0.64

N=3 for all standard deviations.

* represents statistical difference (p < 0.05) in the enrichment factor (Figure 3).

EF can be calculated as shown by equation 2.1. The UCC ratio used in this calculation were determined by measuring the natural abundance of elements in sedimentary rocks (Taylor and Mclennan 1995).

$$Enrichment\ Factor = \frac{\frac{[M]_{sample}}{[Al]_{sanple}}}{\frac{[M]_{UCC}}{[Al]_{UCC}}} \qquad (Equation\ 2.1)$$

There is significant enrichment of several trace metals such as antimony (Sb) and cadmium (Cd). This is expected from an urban area as automobile brake dust is a common source of Sb, and Cd has been linked to numerous urban sources (Lough et al. 2005; Majestic et al. 2009a; Saffari et al. 2013). One compelling observation made from Figure 2.3 is that the enrichment factor for all elements is highest for the samples collected on the train. A few exceptions are Fe, Ba, and As where the enrichment factors were similar for samples collected on board and track-side, but still greater than the urban background found at the CAMP site. The enrichment factors for copper at the downtown site and on board the trains were very similar as well. The fact that the enrichment factors are higher on board the trains is interesting because the overall $PM_{2.5}$ concentrations on the trains were over two times smaller than those at the other site (Figure 2.2).

In order to further investigate this observation, the masses of all elements measured were summed and divided by the overall sample mass. It was determined that the measured metals, those shown in Table 2.1, made up $(25 \pm 10)\%$ of the sample mass, 1400 ± 700 ng m^{-3} collected on board the trains. These metals only contributed $(9.6 \pm 2.4)\%$ of the total sample mass, 1100 ± 400 ng m^{-3}, at the downtown site. The track-side
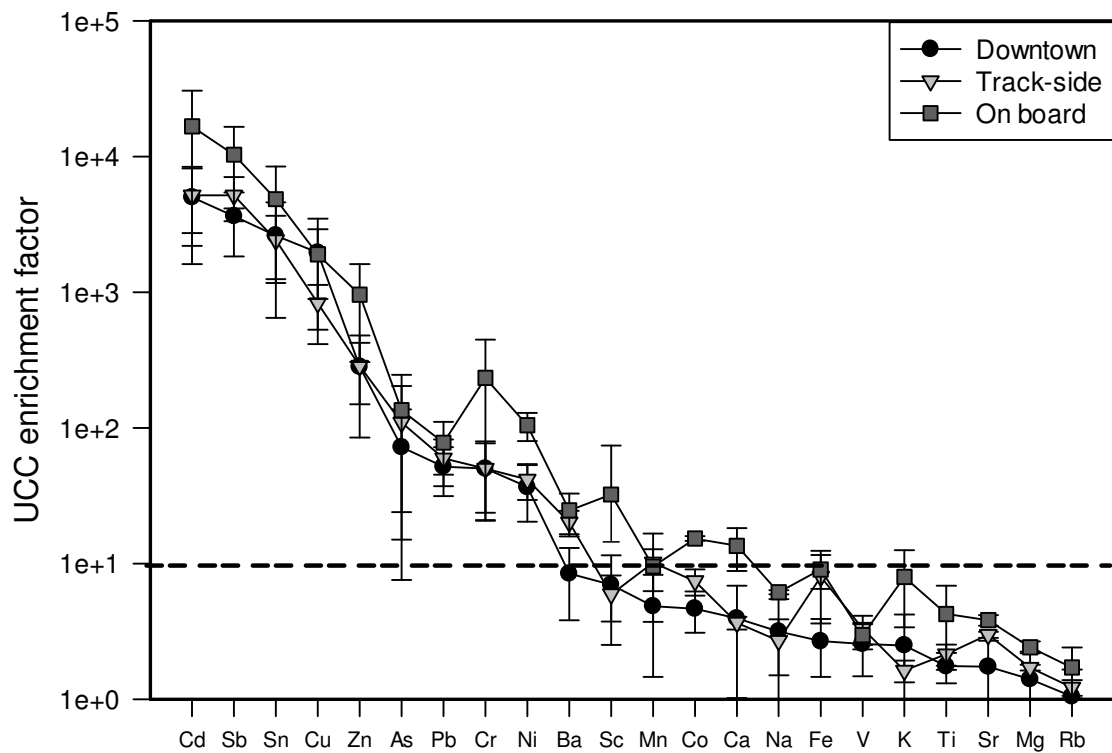
Figure 2.3: UCC enrichment factors for the fine PM at all three sites. Dashed line represents an EF of 10. Elements above that line are dominated by anthropogenic sources.

location had the smallest mass percent of metals in the PM at $(7 \pm 3)\%$, 900 ± 70 ng m^{-3}. It is possible that the higher elemental concentration in the samples collected on board the trains is a result of these samples being collected in an enclosed environment which allowed the elements to become more concentrated unlike at the other sites.

Since soluble metals are more often linked to the adverse health effects of metals in PM, soluble metal concentrations were also determined. Figure 2.4 shows the percent solubility of selected trace elements that exhibited noticeable solubility. In most cases, the percent solubility of the selected elements were statistically similar at all three sites. Notable exceptions are the Zn, As, and Sb which exhibited lower percent solubility in the samples collected on board the trains. In these cases, the percent solubility is noticeably lower than those in the samples collected downtown or track-side.

The speciation of the soluble Fe was also investigated and is shown in Figure 2.5 separated by particle size. It can be seen that Fe(II) comprised the overwhelming majority of the Fe present in the soluble fraction. Soluble Fe concentrations downtown were 29 ± 26 ng m^{-3} or $(14 \pm 10)\%$ of the Fe collected. Track-side soluble Fe concentrations were similar to that of the samples collected downtown at 28 ± 6 ng m^{-3} but only $(7.9 \pm 0.9)\%$ of the total Fe collected. The samples collected on board the trains also contained similar concentrations of soluble Fe, 23 ± 16 ng m^{-3} or $(10 \pm 9)\%$ of the total Fe in the sample. Of the soluble Fe, 87-90% of the Fe was present as Fe(II) across all three locations. The percent solubility of Fe has been studied on a global scale and has been determined to be 0.5-2% for Fe originating from crustal sources; the Fe percent

solubility measured in this study is much greater than that (Sholkovitz et al. 2012), indicating a significant presence of anthropogenically produced Fe at all sites.

2.5 Discussion

Both ground-level and underground rail systems have been previously linked to increased concentrations of metals in $PM_{2.5}$. The overwhelming majority of these studies have focused on underground subway systems (Furuya et al. 2001; Chan et al. 2002; Chillrud et al. 2003; Johansson and Johansson 2003; Aarnio et al. 2005; Chillrud et al. 2005; Karlsson et al. 2005; Seaton et al. 2005; Salma et al. 2007; Mugica-Alvarez et al. 2012; Querol et al. 2012), with only a few studies including ground-level light rail (Adams et al. 2001; Chan et al. 2002; Kam et al. 2011b; Kam et al. 2013). Also, the present study is the first study to measure soluble Fe speciation in samples collected from railway sources as well as in the Denver-Metropolitan area. A number of researchers have presented $PM_{2.5}$ concentrations for samples collected inside the train cabins on both underground and ground-level rail systems (Adams et al. 2001; Chan et al. 2002; Aarnio et al. 2005; Kim et al. 2008; Cheng and Lin 2010; Kam et al. 2011a; Querol et al. 2012; Kim et al. 2014). The average $PM_{2.5}$ concentrations for samples collected in the trains ranged from 11 $\mu g\ m^{-3}$ in Barcelona (Querol et al. 2012) to 247 $\mu g\ m^{-3}$ in London (Adams et al. 2001). When only considering ground level trains the range of average $PM_{2.5}$ concentrations is 14 $\mu g\ m^{-3}$ in Los Angeles (Kam et al. 2011a) to 46 $\mu g\ m^{-3}$ in Hong Kong (Chan et al. 2002). The $PM_{2.5}$ concentration in samples collected on board the trains in the present study are far less than those reported elsewhere at 5.6 ± 1.8 $\mu g\ m^{-3}$

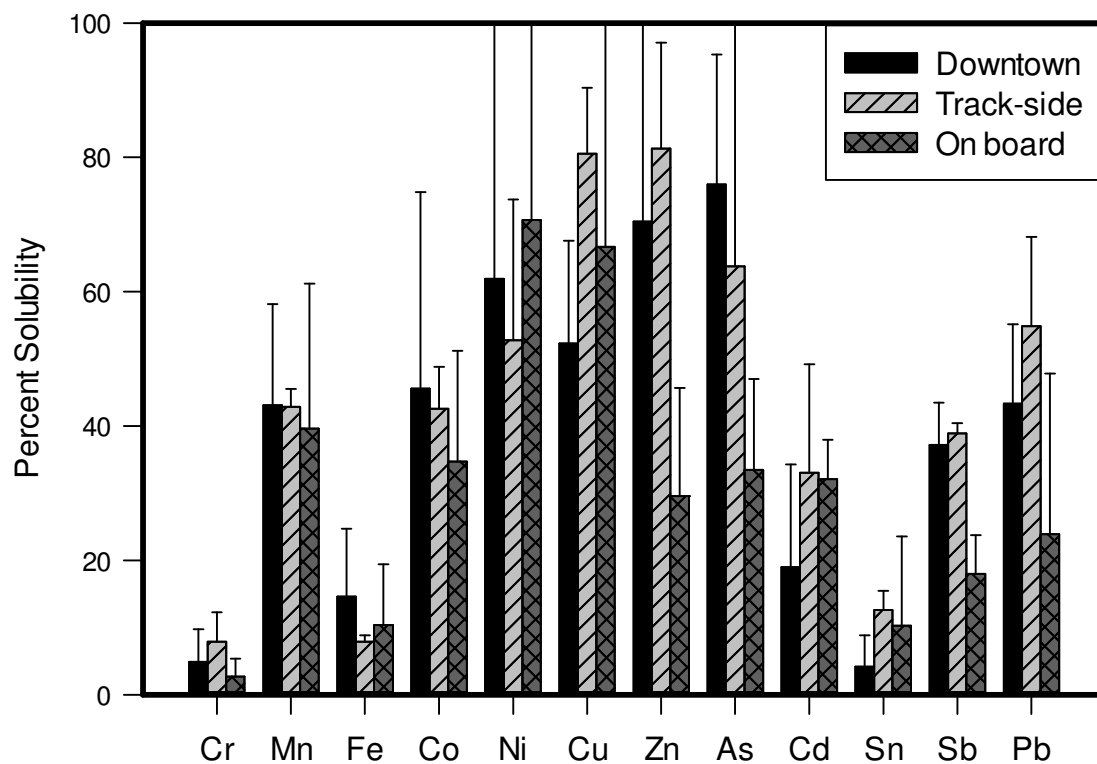**Figure 2.4:** Average percent solubility of select trace elements. Elements were extracted from the sample in a pH 4.25 acetate buffer. Error bars represent the standard deviation of percent solubility.
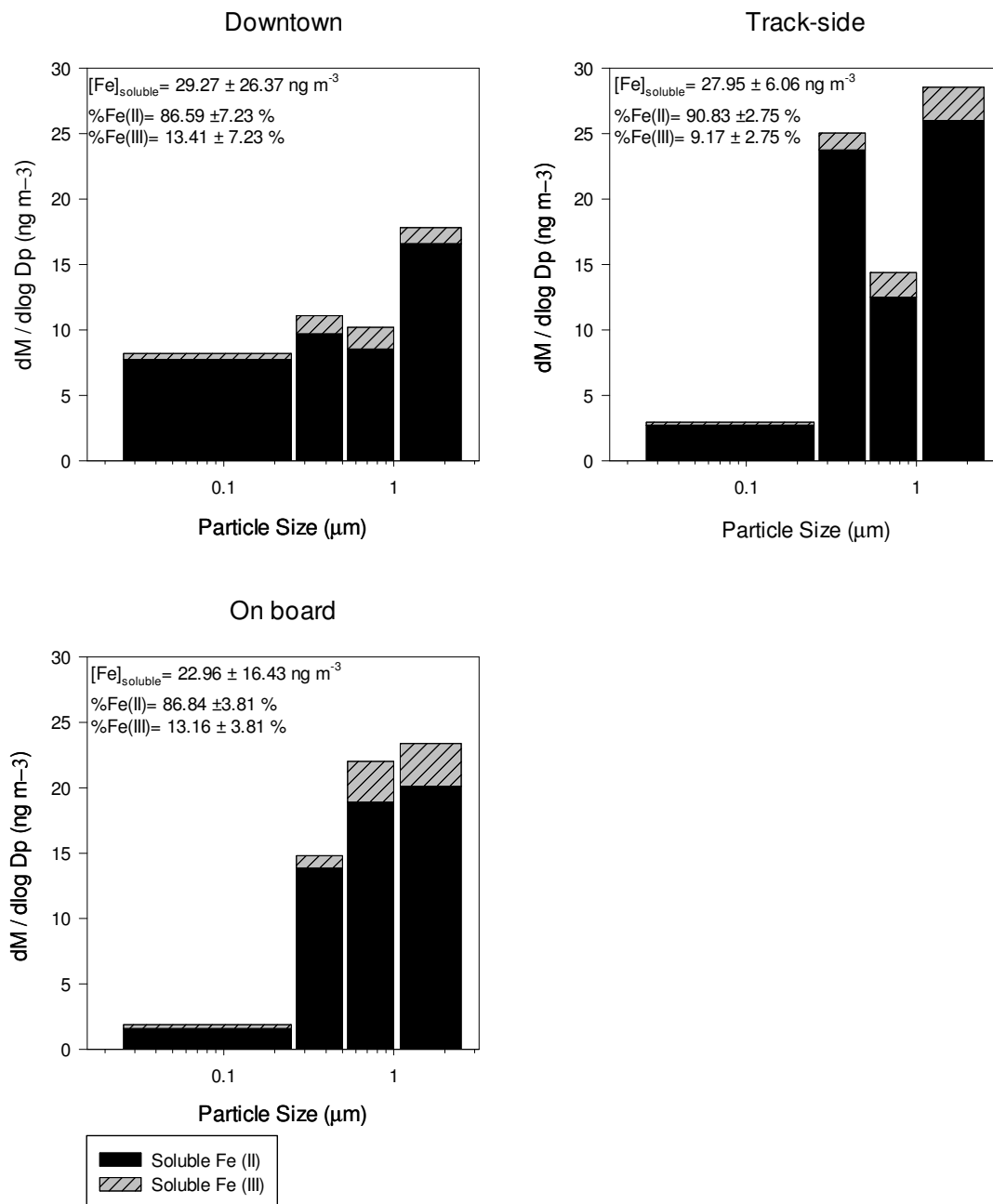
Figure 2.5: Average size-segregated soluble fractions of Fe(II) and Fe(III) at all sampling locations. % Fe(II) and % Fe(III) are the percentages of Fe(II) and Fe(III) in the soluble fraction.

which could be explained by the RTD light rail in Denver being newer than many other rail systems as its operations began in 1994.

Comparatively, the data from this study showed similar results in trace element concentrations in $PM_{2.5}$ as those studies that included ground-level light rail. Also, enrichment of certain trace elements as related to train activity were similar between studies as well. Figure 2.6 shows a comparison of the results from this study with those published by Kam et al. (2011b) from Los Angeles. With the exception of Fe which was measured at higher concentrations in Los Angeles, the concentrations of the metals were equal to or less than the samples collected at all sites in this study. While this shows many similarities between Denver and Los Angeles, it is important to note that direct comparisons between the two cities cannot be made as the rail systems are unique to each city and not all of the measured PM is a result of light rail activity.

Previous studies have suggested that many of these elements related to steel such as Fe, Mn, and Cr are enriched in PM_{10} and $PM_{2.5}$ from rail systems through frictional wearing of the rails and components of the train cars such as wheels and brakes (Chillrud et al. 2003; Chillrud et al. 2005; Kam et al. 2011b). The results from this study (Table 2.1) also show enrichment of Fe above the background at both the track-side site and on board the trains. Mn was shown to be enriched at the track-side site while Cr was enriched in the samples collected on board the train. Ni, another common element in steel was also enriched in the on board samples. Mo, also found in steel, was measured

27

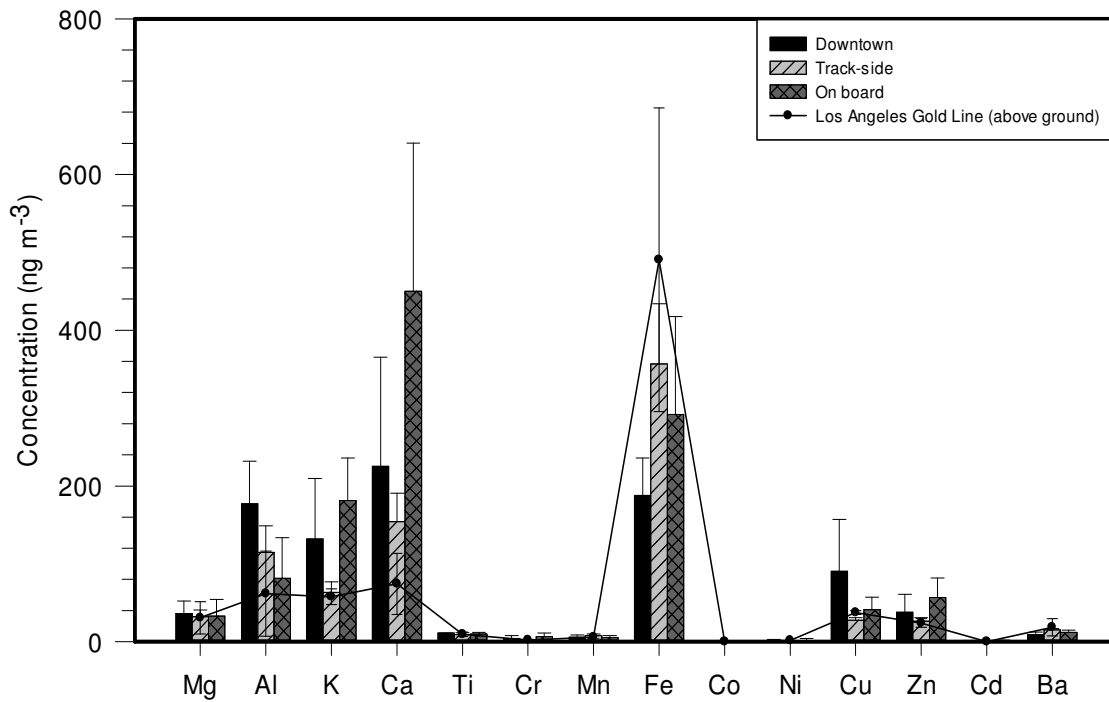**Figure 2.6:** Total metal concentrations at each site. The line represents the concentration of the different metals collected along the Los Angeles Gold Line, an above ground train (Kam et al. 2011b).

and shown to be enriched in the samples collected on board. While PM from frictional processes has commonly been associated with PM_{10}, several of the previous studies regarding railway transportation systems have shown increases in $PM_{2.5}$ above street-level and background locations (Furuya et al. 2001; Johansson and Johansson 2003; Aarnio et al. 2005; Kam et al. 2011b; Mugica-Alvarez et al. 2012; Kam et al. 2013). $PM_{2.5}$ and PM_{10} have been found to be highly correlated in Los Angeles suggesting similar sources (Kam et al. 2011a). This is further supported by the presence of a significant ultrafine mode resulting from brake wear (Garg et al. 2000). Also, $PM_{2.5}$ has been shown to have a greater impact than coarse particles on the negative health effects associated with the inhalation of PM (Pope and Dockery 2006; Hu et al. 2008).

The EF for all of the measured elements was highest in the samples collected on board the train. This can be explained by the resuspension of $PM_{2.5}$ by foot traffic through the train. Several studies have shown that walking will resuspend particles with the bulk of the resuspended particles being in the coarse mode. However, these studies have also shown that the coarse particles will deposit faster than the fine particles (Montoya and Hildemann 2005; Rosati et al. 2008; Cheng et al. 2010). As a result, it can be posited that continual respuspension of $PM_{2.5}$ could increase enrichment of fine trace metals in the samples collected on board the train.

The cause for the observed increase in Ca in samples collected on board the trains over samples collected downtown and track-side is not fully known. As can be seen in Figure 2.3, Ca was shown to have a higher enrichment factor in the samples onboard the train suggesting that the Ca concentration was influenced by anthropogenic activities (EF

29

>10). A potential source of Ca could be calcium hypochlorite, a common disinfectant that could be used in cleaning supplies used to clean the interior surfaces of the trains.

While this is the first study to measure Fe speciation and solubility in Denver, CO, Fe speciation studies in Los Angeles, CA and East St. Louis, IL have shown that Fe(III) is the predominant Fe species in atmospheric PM while Fe(II) is the predominant soluble Fe species (Majestic et al. 2007a). The Fe solubility results in this study were similar to these other studies with 87-90% of the soluble Fe being Fe(II) and soluble Fe(II) also comprising 7-14% of the total Fe (Majestic et al. 2007a; Oakes et al. 2012b). The measured percent Fe(II) of soluble Fe in this study and the results for Los Angeles and East St. Louis from the study by Majestic et al. (2007a) are larger than results reported for Waukesha, WI where the percentage of soluble Fe(II) was found to be 50% (Majestic et al. 2007a) as well as the results reported for urban Atlanta, GA where the percentage of Fe(II) in the soluble Fe ranged from 31% to 88% (Oakes et al. 2012b). In both studies, Majestic et al. (2007a) and Oakes et al. (2012b), higher concentrations of soluble Fe(II) were measured in the winter time, a similar time period as the collection period of this study. Similarly, urban areas have been shown to have elevated soluble Fe.

This is important as soluble Fe has been directly correlated to ROS production (Kam et al. 2011b). Fe(II) has also been correlated with the reduction of hydrogen peroxide to form the hydroxyl radical (Halliwell and Gutteridge 1986). Other soluble trace metals of note in this study that have been found to form ROS in other studies are Cr, Ni,(Kam et al. 2011b) and Cu (DiStefano et al. 2009). Cr is also known to be

particularly toxic based on speciation and has also been studied in railway transportation systems (Salma et al. 2009).

2.6 Conclusions

The results of this study provide interesting insights into the effects of light rail activity in the Denver-Metropolitan area. While the air near the tracks or on board the train may not contain more $PM_{2.5}$ than that of the ambient air in Denver, it is important to note that there is definite enrichment of trace metals on board the train and near the tracks. These results have also shown that the $PM_{2.5}$ collected on board the trains was composed of 25% (by mass) metals while the $PM_{2.5}$ collected at the other two sites was less than 10%. Future studies could focus on the seasonal variability of metal concentrations in the Denver-Metropolitan area as well as investigate the difference in $PM_{2.5}$ composition and concentration on each train line individually.

2.7 Acknowledgements

Chapter Three: The impact of particle size, relative humidity, and sulfur dioxide on iron solubility in simulated atmospheric marine aerosols*

3.1 Abstract

Iron is a limiting nutrient in about half of the world's oceans, with its most significant source being atmospheric deposition. To understand the pathways of iron solubilization during atmospheric transport, size segregated simulated marine aerosols were exposed to 5 ppm sulfur dioxide at arid (23 ± 1% RH) and marine (98 ± 1% RH) conditions. Relative iron solubility increased as the particle size decreased for goethite and hematite, while for magnetite, the relative solubility was similar for all of the fine size fractions (2.5-0.25 µm) investigated but higher than the coarse size fraction (10-2.5 µm). Goethite and hematite showed increased solubility at arid RH, but no difference (p>0.05) was observed between the two humidity levels for magnetite. There was no correlation between iron solubility and exposure to SO_2 in any mineral for any size fraction. X-ray absorption near edge structure (XANES) measurements showed no change in iron speciation [Fe(II) and Fe(III)] in any minerals following SO_2 exposure. SEM-EDS measurements of SO_2-exposed goethite revealed small amounts of sulfur uptake on the samples, however, the incorporated sulfur did not affect iron solubility. These results show that, although sulfur is incorporated into particles via gas-phase processes, changes in iron solubility also depends on other species in the aerosol.

3.2 Introduction

Iron is the most abundant transition element in the atmosphere and the Earth's crust. Iron concentrations in marine air have been measured at 200-500 ng m^{-3} and as high as >10,000 ng m^{-3} during Asian dust storms (Johansen et al. 2000b; Chuang et al. 2005). Globally, the iron concentration in atmospheric PM ranges from 5-17,000 ng m^{-3}, with the lowest concentrations found in remote regions of the Atlantic and Pacific Oceans (Mead et al. 2013) and highest concentrations found off the coasts of South Korea and West Africa (Bowie et al. 2009; Sholkovitz et al. 2012). The dominant source of iron to the marine atmosphere is wind-blown dust from the erosion of continental soils (Jickells and Spokes 2001; Jickells et al. 2005; Mahowald et al. 2009); however, anthropogenic sources such as motor vehicles (Lough et al. 2005), and industrial processes (Luo et al. 2008; Majestic et al. 2009b) have also been shown to contribute iron to the atmosphere. In total, it has been estimated that 14-16 Tg of iron is deposited annually into the ocean, most of which originates from desert areas (Gao et al. 2003; Jickells et al. 2005).

The deposition of atmospheric iron into the ocean is important as iron is known to be a limiting micronutrient to phytoplankton in the open ocean (Boyd et al. 2007). Despite such a large amount of iron being deposited into the ocean, the iron is only marginally soluble, 0.5-2%, in seawater (Chen et al. 2006; Wu et al. 2007; Ooki et al. 2009; Aguilar-Islas et al. 2010; Buck et al. 2010b; Sholkovitz et al. 2012). However, fractional solubility in dust has been shown to increase to more than 50% over the ocean (Zhuang et al. 1992). There are numerous potential explanations of the increased soluble iron including 1) the effects of particle size (Baker and Jickells 2006; Ooki et al. 2009),

2) the ability of particles to serve as cloud condensation nuclei (Spokes et al. 1994), 3) aerosol acidification and reactions during the transport, especially those involving anthropogenic gases such as sulfur dioxide (SO_2) (Baltrusaitis et al. 2007; Cwiertny et al. 2008; Duvall et al. 2008; Chen and Grassian 2013; Ito and Xu 2014; Kong et al. 2014), 4) the mineralogy of the source of the dust (Journet et al. 2008), and 5) the mixing of anthropogenic iron with iron in lithogenic dust (Luo et al. 2008; Mahowald et al. 2009; Sholkovitz et al. 2009; Sholkovitz et al. 2012).

Previous work (Baker and Jickells 2006; Ooki et al. 2009) found that higher iron solubility was observed for fine mode aerosols rather than coarse mode. Baker and Jickells hypothesize that this was a result of particle solubility being a surface process and as particles become smaller a greater relative surface area is available for dissolution. Conversely, Buck et al. (2010a) found that iron solubility in marine aerosols collected over the Atlantic Ocean tended to be higher in particles in the larger size fractions which were studied. This discrepancy in results from ambient data highlights the need for a well-defined laboratory study. Since smaller particles are transported further from the source (larger particles are likely to settle), it is expected that particles being deposited into the open ocean will be smaller particles with more surface reaction sites. Similarly, increased relative humidity (RH), such as that in a marine environment, could lead to particle dissolution via aqueous processes during transport over the ocean as salts, e.g. sodium chloride (NaCl), begin to deliquesce at 76% RH (Pilinis et al. 1989). Condensation and particle dissolution during transport can also allow for the interaction of particulate iron with other chemical species such as SO_2.

SO$_2$ is a common anthropogenic air pollutant that has been shown to be at greater concentrations in urban air, 20-30 ppb, than in the marine atmosphere, 0.03-1 ppb (Meskhidze et al. 2003). Under atmospheric conditions, SO$_2$ is oxidized to sulfuric acid (Finlayson-Pitts and Pitts Jr 2000; Seinfeld and Pandis 2006) which leads to particle acidification and may lead to greater iron solubilization (Chen and Grassian 2013). Iron, especially Fe(III), in the aqueous phase has also been shown to catalyze the oxidization of SO$_2$ to sulfate (Faust and Hoffmann 1986; Harris et al. 2012; Harris et al. 2013). Subsequently, this oxidation leads to the formation of Fe(II), a more soluble form of iron (Majestic et al. 2006; Majestic et al. 2007a). In addition to aqueous chemistry, heterogeneous (i.e. gas-particle) chemistry may also be an important route to iron solubilization as iron-containing dust originates in arid regions and can then be transported over urban areas leading to interactions with SO$_2$. The heterogeneous uptake of SO$_2$ on hematite has been observed, especially in the presence of nitrate (Kong et al. 2014), further suggesting the importance of investigating gas-particle phase chemistry in terms of iron solubilization. Oakes et al. (2012a) found a relationship between iron solubility and particle sulfate content. It was reported that a decrease in the iron:sulfate ratio corresponded to an increase in iron solubility for source emissions, however this trend was not reciprocated in ambient PM$_{2.5}$ collected in Atlanta, GA, USA. Luo et al. (2005) found no correlation between simulated SO$_2$ processing and iron solubility from a global data set. These discrepancies in the effects of SO$_2$ on iron solubility, again, further highlight the need for controlled laboratory experiments.

Mineralogy of atmospheric dust has also been shown to have a significant impact on iron solubility. Numerous studies have reported increased iron solubility as a result of iron-containing clay minerals (e.g. illite) present in the aerosols (Cwiertny et al. 2008; Journet et al. 2008; Deboudt et al. 2012; Jeong and Achterberg 2014). Journet et al. (2008) report that iron solubility in clay was ~4% while iron (oxyhydr-)oxides (e.g. hematite, goethite, and magnetite) were <1% and that 90% of soluble iron was from iron-containing clays rather than iron (oxyhydr-)oxides, however the particle size was not reported. Other studies have suggested a significant impact of iron (oxyhdr-)oxides, especially the involvement of these minerals in the adsorption of SO_2, however those studies have not used simulated aerosols in controlled laboratory conditions (Baltrusaitis et al. 2007; Deboudt et al. 2012; Kong et al. 2014).

In this study, laboratory-based experiments were used to investigate both aqueous and heterogeneous processes which may solubilize atmospheric iron present in simulated aerosols (Figure 3.1). Mixed iron mineral and NaCl samples were exposed to SO_2 at marine and arid RH levels in order to further elucidate the effects of these variables on the solubilization of particulate iron. Iron solubility was measured using inductively-coupled plasma mass spectrometry (ICP-MS), while changes in chemical speciation [i.e. Fe(II) and Fe(III)], uptake of sulfur, and other physical changes were monitored using x-ray absorption near edge structure (XANES) spectroscopy and scanning electron microscopy-energy dispersive x-ray spectroscopy (SEM-EDS).
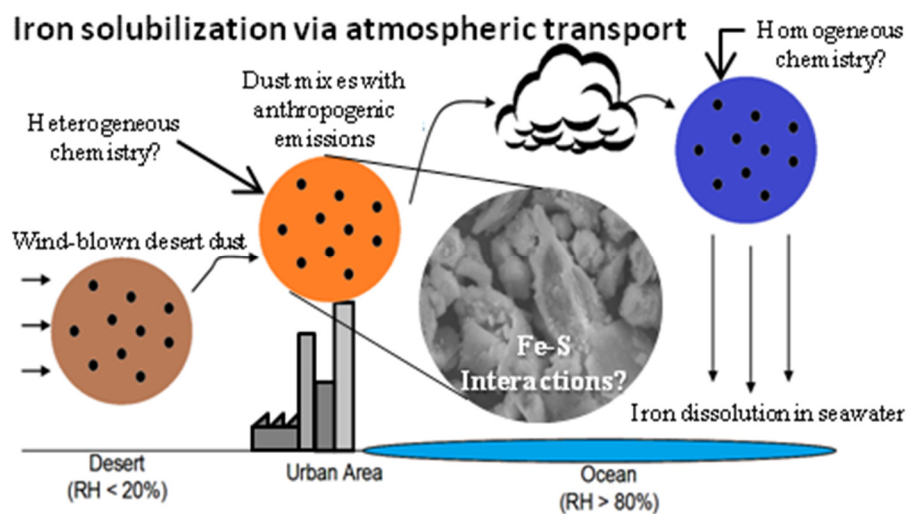
Figure 3.1: Graphic depicting hypothesized iron solubilization through atmospheric transport and the areas studied in this chapter.

3.3 Materials and Methods

3.3.1 Sample preparation

Hematite (Fe_2O_3), magnetite (Fe_3O_4, American Education Products), goethite

(FeOOH), and illite (an iron containing clay;

$(K,H_3O)(Al,Mg,Fe)_2(Si,Al)_4O_{10}[(OH)_2,(H_2O)]$, Ward's Natural Science) were mixed with

NaCl at a molar ratio of 4:1 Na:Fe and then ground using a ball-mill. A 4:1 Na:Fe

mixture was used to simulate the chemical composition of PM over the oceans (Johansen

et al. 2000b). NaCl was also used to simulate marine aerosols and induce deliquescence

at marine level RH and allow for potential homogeneous chemistry to take place.

Ground and mixed samples were resuspended and separated by aerodynamic size (10-2.5,

2.5-1, 1-0.5, 0.5-0.25, and <0.25 μm) using a Sioutas Personal Cascade Impactor Sampler

(PCIS, SKC Inc.) at 9 L min^{-1} (Misra et al. 2002; Singh et al. 2003; Carvacho et al. 2004).

Samples were collected on acid-washed Teflon collection substrates for the largest four

size fractions (0.5 μm pore size 25 mm Zefluor, Pall Life Sciences) filters, while 2.0 μm

pore size 37 mm Teflo (Pall Life Sciences) filters were used for the smallest size fraction.

Goethite samples were also collected on aluminum substrates used for SEM analysis;

however the final catch stage is flow through, and thus cannot be an impaction stage. Per

filter, sample masses ranged from 3-1000 μg for iron (oxyhydr-)oxides and 100-3500 μg

for illite clay, with the lower end of the masses generally present on the smaller size

fractions.

3.3.2 Exposure methods

Each size fraction of the iron mineral:NaCl mixture was exposed to four environments: 1) marine level RH with SO_2, 2) marine RH without SO_2, 3) arid RH with SO_2, and 4) arid RH without SO_2. Samples were exposed in two polypropylene vacuum desiccators (Scienceware) for 27 hours. This time scale was chosen to represent a 24 hour cycle and to allow for three hours of equilibration. In order to increase the RH inside the chambers to marine levels, a supersaturated solution of potassium nitrate was used (Pilinis et al. 1989), where the RH was $98 \pm 1\%$. For simulating an arid environment, a desiccant (Drierite) was used to maintain RH at $23 \pm 1\%$. Temperatures were all ambient laboratory temperatures ($20 \pm 3\,°C$). For SO_2 exposure, the ambient air was removed with a vacuum pump and the chamber was pressurized to ambient pressure (~103 kPa) with a 5 ppm SO_2 in air mixture (Air Liquide). It should be noted that this concentration of SO_2 is approximately 10000x higher than ambient SO_2 concentrations (Meskhidze et al. 2003). Radical chemistry was not explored in this study and care was taken to avoid possible radical formation by not exposing samples to ultraviolet radiation thus minimizing potential photocatalysis. To perform multiple analyses on one filter, each sample filter was cut into thirds. One third of the sample was exposed to SO_2 at either high or low humidity; one third was only exposed at the particular humidity level with no SO_2, while the final third was used for total iron determination.

3.3.3 Total iron determination

Dissolution of the sample was achieved using a microwave digestion system (Ethos EZ, Milestone, Inc). Samples (one third of a filter) were digested in a Teflon vial

using 750 µl nitric acid (Fisher) and 250 µl hydrochloric acid (Fisher). All acids were trace-metal grade purity. Samples were digested in 6 mL Teflon vessels following a temperature program of a 9 minute ramp to 180 °C, a hold at 180 °C for 10 minutes, and a 60 minute cool-down period. Following digestion, samples were diluted to 15 mL using Milli-Q (18.2 MΩ-cm) water and analyzed via quadrupole ICP-MS (Agilent 7700) using indium as internal standard and a He collision cell to remove polyatomic interferences, particularly $^{40}Ar^{16}O^+$. The ICP-MS method detection limit for iron was 0.04 µg L^{-1}. All sample preparation was performed under HEPA-filtered air laminar flow hoods.

3.3.4 Soluble Iron Determination

For soluble iron analysis, each exposed sample was extracted in 10 mL of a simulated cloud water buffer (pH = 4.25) for two hours. The buffer consisted of 0.5 mM acetate, 0.5 mM formate, and 0.2 mM ammonium nitrate (Siefert et al. 1996; Baker and Jickells 2006; Upadhyay et al. 2011) and the pH of the extract remained within 4.25 ± 0.01 over the course of the extraction (Accumet Basic AB 15, Fisher Scientific). The extracts were then filtered (0.2 µm, Whatman), acidified to 3% with HNO_3, and total soluble iron was analyzed using ICP-MS.

3.3.5 XANES and SEM-EDS Measurements

XANES data was collected at the Advanced Light Source MicroXAS beamline (10.3.2) at the Lawrence Berkeley National Laboratory, Berkeley, CA, USA. K-edge energy values were used for the determination of changes in iron speciation as a result of exposure to SO_2. SEM-EDS measurements were used to explore morphological changes

to the iron phases after SO_2 exposure. A JEOL JSM-7000F Field Emission Scanning

Electron Microscope was used at Colorado School of Mines, Golden, CO, USA.

3.4 Results

Figure 3.2 shows the results of the SO_2 and RH solubility experiments for the

minerals of the four larger aerodynamic sizes: 10-2.5, 2.5-1, 1-0.5, and 0.5-0.25 µm.

The results for particles of aerodynamic size <0.25 µm are not shown because the sample

mass was too low. The results for illite are also not shown due to large uncertainty

because of sample loss while the filters were cut. Sample loss during filter cutting was

not observed for the hematite, goethite, and magnetite. The relative iron solubility of

hematite and goethite tends to increase as the particle size decreases ($p < 0.05$).

Magnetite, however, showed similar iron solubility for the three smaller size fractions

(2.5-0.25 µm), but the solubility in all of these fractions is greater than in the 10-2.5 µm

fraction ($p < 0.05$). The relative solubility for magnetite and hematite ranged from 0.25-

2.0%, while goethite relative solubility was considerably less ranging from 0.02-0.12%.

For goethite and hematite (Figure 3.2 A and C respectively) the particles exposed to the

arid level RH appear to show higher relative solubility than those exposed at the marine

level RH, however these differences were not significant ($p > 0.05$). For magnetite

(Figure 3.2 B), there was also no difference ($p > 0.05$) between arid and marine RH

conditions. No correlation was found between iron solubility and exposure to SO_2 in any

mineral at any condition. A summary of the statistical comparisons were made between

each factor (particle size, RH, and SO_2) and these results are found in Appendix B. The

results of the statistical tests showed that particle size had the greatest effect on iron
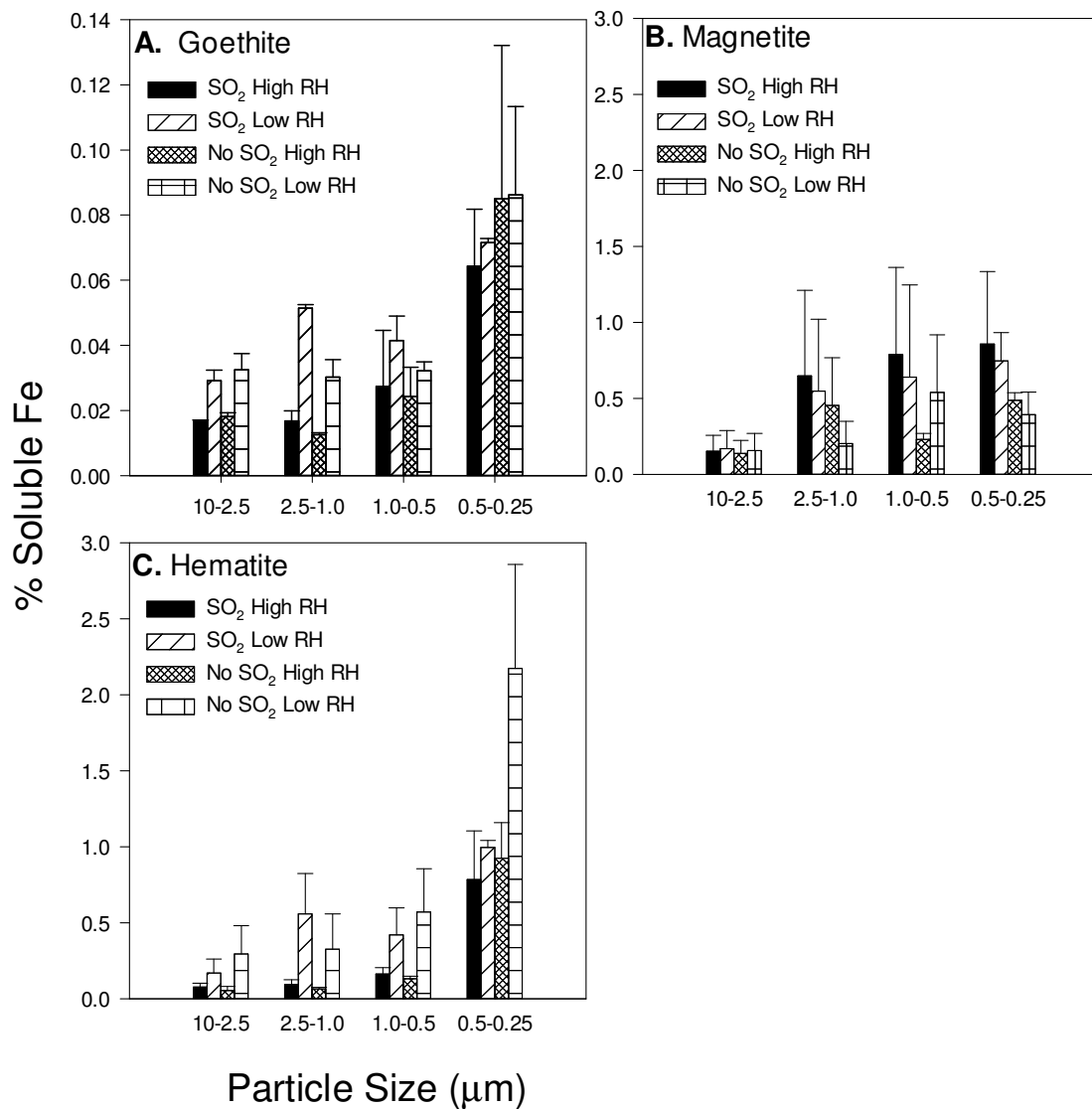
Figure 3.2: Relative iron solubility in goethite (A), magnetite (B), and hematite (C). Error bars (N=2) represent the range.

solubility and that exposure to SO_2 did not result in changes in iron solubility under any measured condition.

Figures 3.3 and 3.4 show the XANES spectra for hematite, magnetite, and illite for the largest size fraction (10-2.5 µm, Figure 3.3) and the smallest size fraction (<0.25 µm, Figure 3.4). In each figure, the K-edge normalized intensity is plotted versus the energy. The solid line in each plot corresponds to the samples not exposed to SO_2 while the circles represent the samples which were exposed to SO_2. The inset for each plot shows the K-edge peak and the corresponding K-edge energy (eV). In each case there was no significant difference in the K-edge values. A significant difference in K-edge energy would suggest a change in oxidation state or coordination chemistry, however, Figures 3.3 and 3.4 both support the findings from Figure 3.2, in that SO_2 had no detectable effect on the chemical speciation of the iron in the samples.

Figures 3.5 and 3.6 show SEM images and EDS spectra for goethite and NaCl mixtures for particles with aerodynamic sizes of 10-2.5 µm and 0.5-0.25 µm, respectively. The smallest particles (<0.25 µm) could not be used as they could not be collected on a conductive, aluminum substrate. In both Figure 3.5 and Figure 3.6, small amounts of sulfur were detected in the samples exposed to 5 ppm SO_2, while none was detected for the samples not exposed to SO_2. A more intense sulfur signal was recorded, at both aerodynamic sizes, for the samples exposed at the marine RH than at the arid RH. This suggests the possibility of homogeneous and heterogeneous processes on the particle, but not necessarily with the iron. Physical changes in the particles were not observed as a result of the exposures. In the SEM images shown in Figure 3.5, large

43
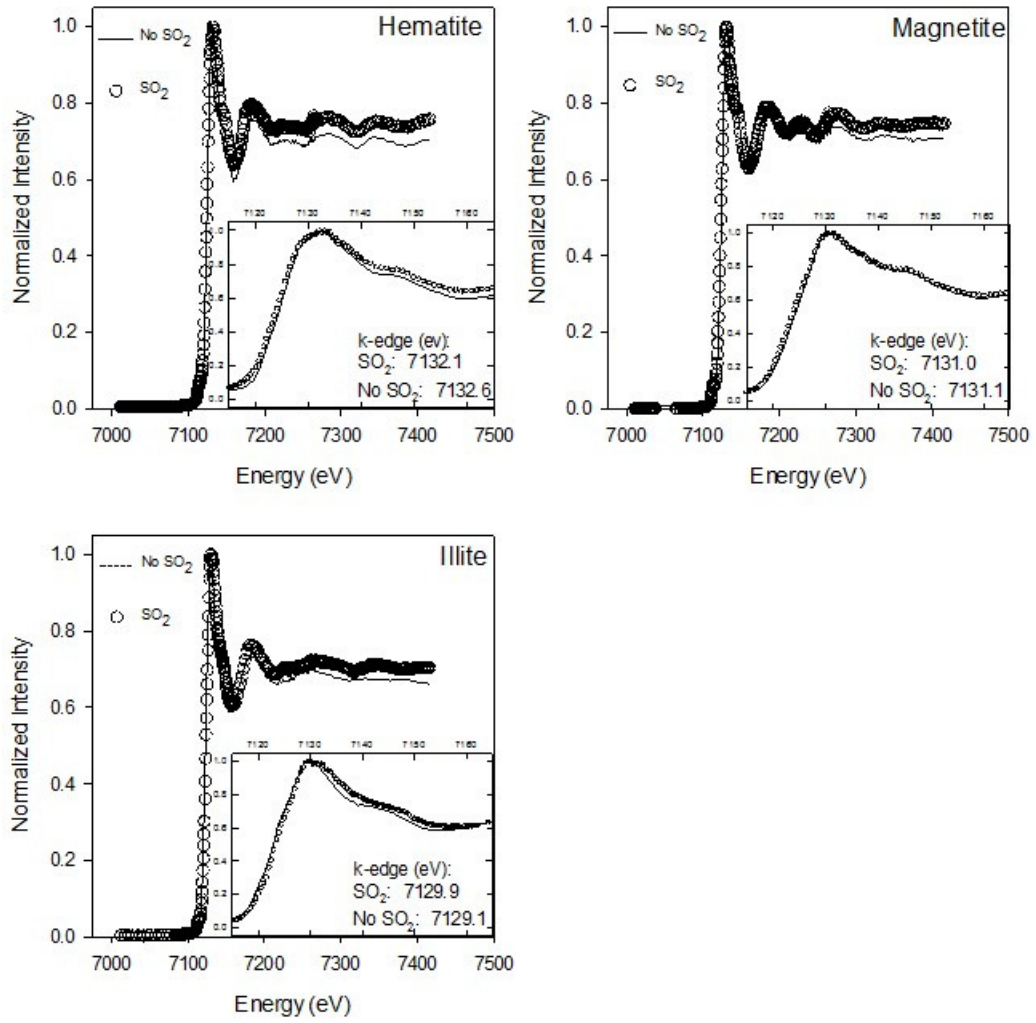
Figure 3.3: XANES spectra of iron minerals. Energy values represent K-edge energies and particle aerodynamic size is 10-2.5 µm. The inset shows the K-edge peaks in greater detail.
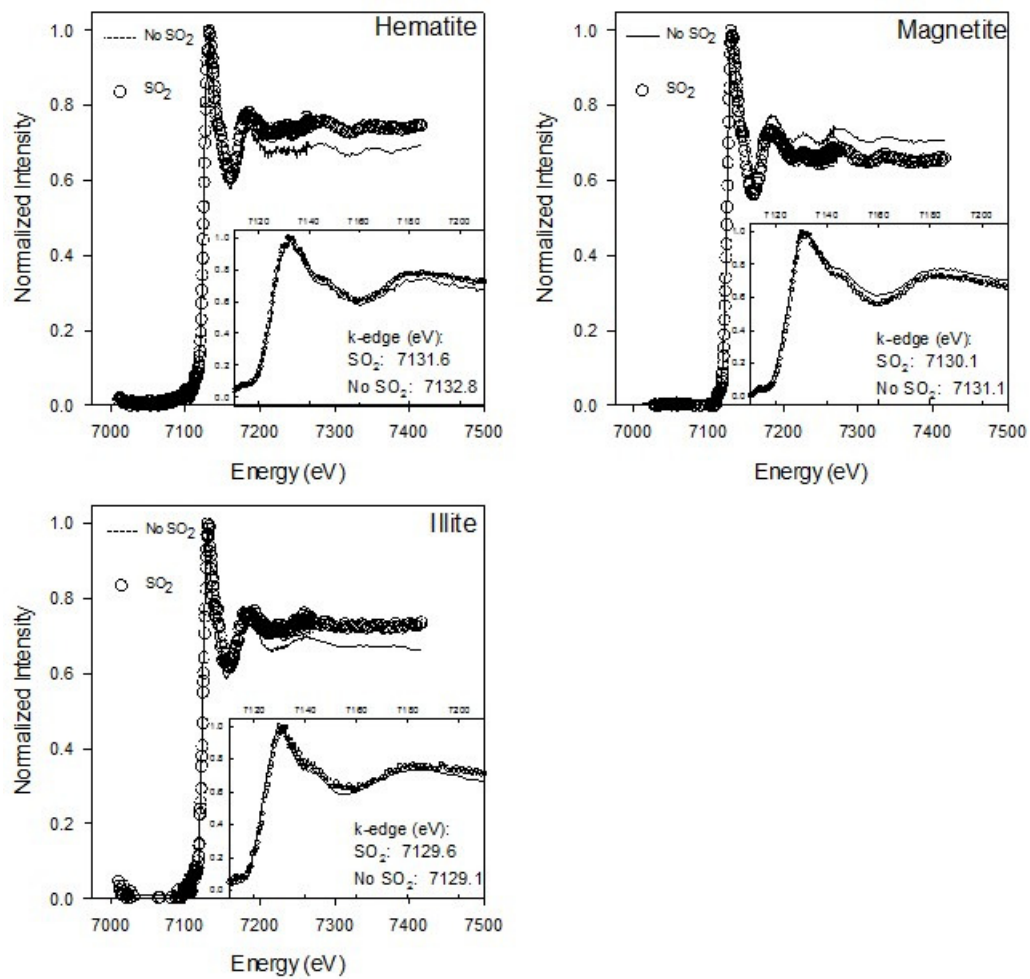
Figure 3.4: XANES spectra of iron minerals. Energy values represent K-edge energies and particle aerodynamic size is <0.25 µm. The inset shows the K-edge peaks in greater detail.
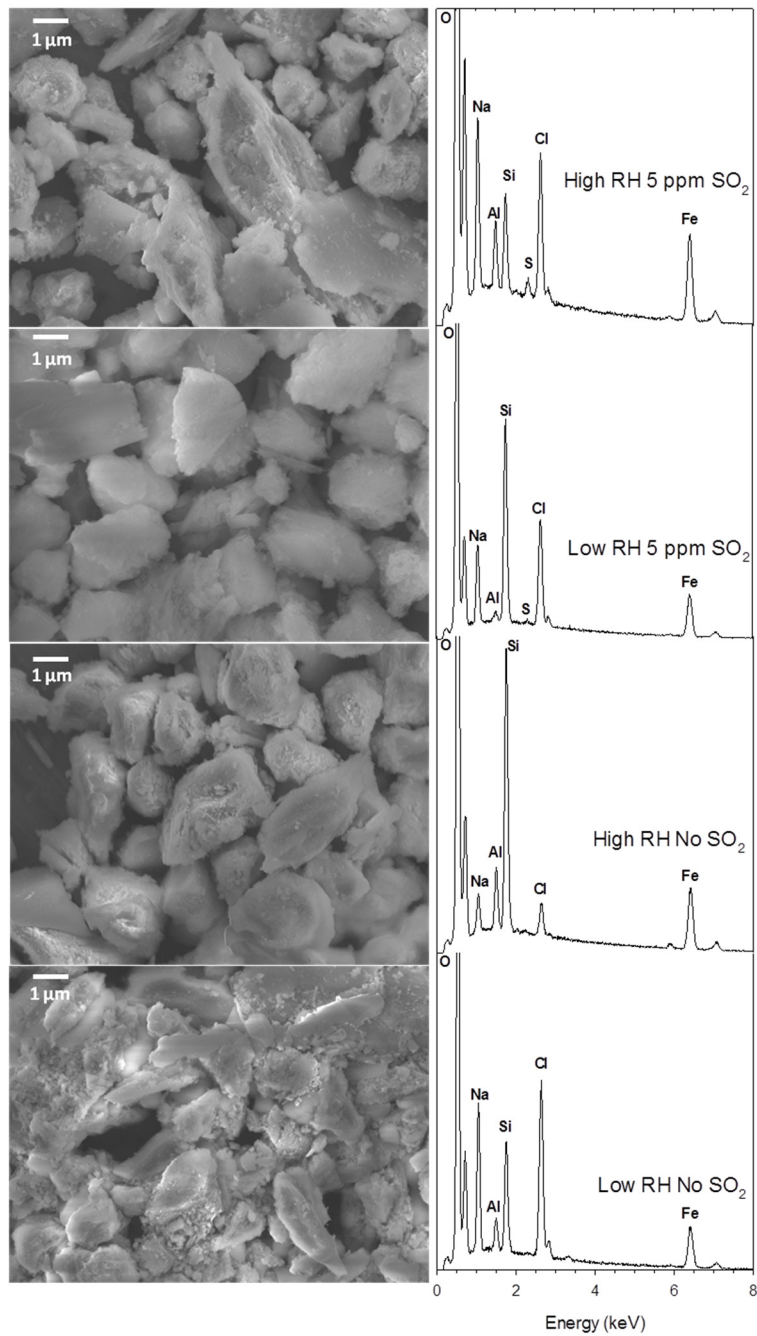
Figure 3.5: SEM images and EDS spectra for goethite-NaCl mixtures exposed at various conditions noted on EDS spectra. Particle aerodynamic size: 10-2.5 μm.
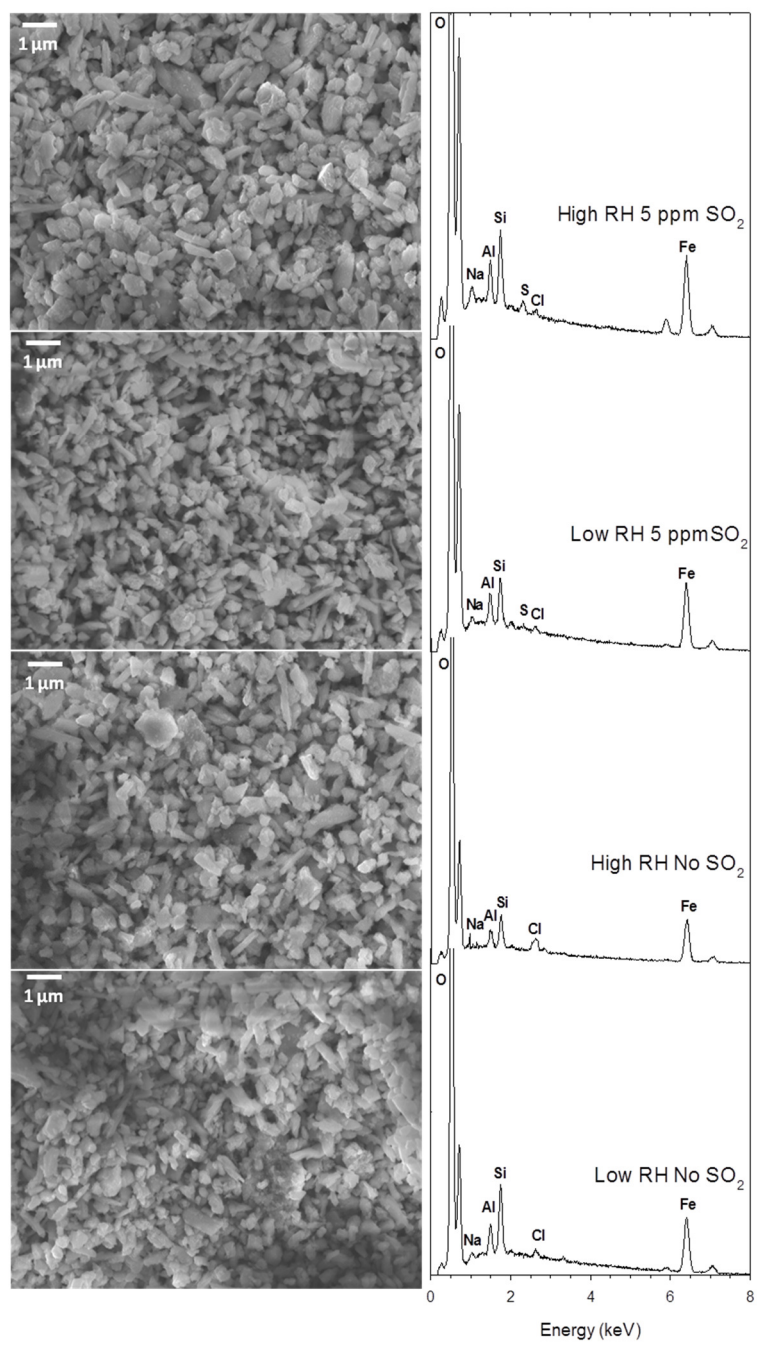
Figure 3.6: SEM images and EDS spectra for goethite-NaCl mixtures exposed at various conditions noted on EDS spectra. Particle aerodynamic size: 0.5-0.25 µm.

rectangular particles can be seen, however after closer inspection with EDS, it was determined that these areas were rich in NaCl suggesting some extent of non-homogeneity in the samples with respect to NaCl concentration. The small amount of sulfur detected in the exposed samples suggests that there is an interaction between the sample and the SO_2 and that higher RH could increase this, however, the solubility data suggest that the effect is too small to have an effect on the measurable iron solubility and mineral chemistry as shown in Figures 3.2-3.4

3.5 Discussion

This study highlights the impacts of different atmospheric conditions on iron mineral:NaCl mixtures and subsequent iron solubility to mimic atmospheric transport from source to deposition. Numerous studies have focused on the effects of different factors on iron solubility but few have measured the combined effects.

The measured relative solubility of iron in this study correlated well with previous studies despite different extraction solutions. Sholkovitz et al. (2012) compiled sets of data on a global scale and determined that relative iron solubility ranged from 0.5-2.0% in aerosols comprised primarily of lithogenic dust. The results from this study showed that iron solubility on native minerals ranged from 0.02-2.0%. Iron solubility is likely lower than the average range due to the lack of mixing with anthropogenic compounds, namely combustion aerosols. Luo et al. (2008), Mahowald et al. (2009), and Sholkovitz et al. (2009) examined the effects of combustion aerosols on iron solubility and determined that mixing of the iron in these anthropogenic aerosols with the iron in lithogenic particles increased the relative iron solubility, sometimes as high as 70-85%

48

(Sholkovitz et al. 2009). Since the particles in this study were prepared to mimic lithogenic particles it makes sense that the iron solubility would be close to the global average.

The increase in relative solubility with a decrease in particle size observed in this study is in agreement with what the majority of other field studies have found. Baker and Jickells (2006) and Ooki et al. (2009) all found that iron solubility was higher in fine particles than in coarse particles, while this study made these observations using well-defined particles in well-defined conditions. Relative iron solubility increased from 0.25-2% for hematite and 0.02-0.13% for goethite as the particle aerodynamic size decreased from 10-2.5 µm to 0.5-0.25 µm. For magnetite the relative iron solubility increased from 0.25-1% between the 10-2.5 µm and 2.5-1.0 µm however, the iron solubility showed no change in the size fractions from 2.5-0.25 µm. This shows a difference between coarse and fine mode particles but not a difference within the fine mode for magnetite particles. This has implications on iron availability because smaller particles are carried further over the ocean with deposition in the open ocean as opposed to coastal areas (Baker and Jickells 2006; Baker and Croot 2010). Deposition of smaller particles with a greater relative solubility effectively increases the bioavailability of iron in remote regions of the ocean. Buck et al. (2010a) observed greater iron solubility in particles with a diameter greater than 1 µm for aerosols collected over the Atlantic Ocean, observing nearly 80% soluble iron in these particles. This could be a result of a mixing of anthropogenic iron with crustal iron as well as mixing of different iron containing minerals.

Mineralogy does have an impact on relative iron solubility. Journet et al. (2008) and Jeong and Achterberg (2014) also suggested mineralogical dependences on iron solubility in iron containing minerals and Asian and Saharan dusts respectively. While Journet et al. (2008) only used iron-containing minerals, the dissolution methods used a highly acidic solution (pH=2) while this study observed the effects of mineralogy on iron solubility in simulated cloud water. Measurements made for iron oxides (hematite and magnetite) corresponded to greater iron solubility than iron oxyhydroxides (goethite) by almost a factor of 10. Also, iron solubility in magnetite did not share the trend of increasing solubility with decreasing particle size as three of the size fractions had similar solubility. This is of particular interest as various dust sources will have differences in mineralogy.

While it was expected that both homogenous and heterogeneous interactions with SO_2 would lead to a change in iron coordination chemistry or iron speciation, the XANES data showed no difference between the SO_2- exposed iron and the iron that was not exposed to SO_2. Although the XANES data did not indicate an interaction between the SO_2 and iron, the SEM-EDS results (Figures 3.5 and 3.6) did show the presence of sulfur in the samples exposed to SO_2. Of particular interest is that the signal intensity of sulfur in the samples exposed to SO_2 at the marine RH was almost three times that of the samples exposed to SO_2 at the arid RH. This suggests that the presence of water on the particles, as a result of deliquescence of NaCl at marine RH, leads to increased opportunity for the uptake of sulfur. However, the XANES data shows that this small amount of sulfur did not affect iron speciation, which was also supported by the iron

solubility experiments. This suggests that, although S was taken up, it was likely associating with the NaCl and not the iron. Kong et al. (2014) observed changes at the particle surface of hematite particles exposed to SO_2 which were correlated to sulfate formation on the particle which was detected in EDS measurements. These changes were also observed, albeit to a lesser extent, on the particles exposed at marine RH and to SO_2 (Figure 3.5, top image). Areas that corresponded to higher amounts of NaCl also corresponded to a higher weight percent of sulfur. This supports an interaction of the sulfur with the NaCl in the sample. It has been shown that sulfur can displace chloride in atmospheric particles (Johansen et al. 2000b), resulting in minimal interaction with iron.

This study shows that mineralogy and particle size are the most important factors impacting iron solubility in atmospheric particles and that SO_2 plays a very limited role in iron solubility. Factors not considered here, such as organic complexation, photochemical and radical pathways, may still be important and warrant further study (Paris et al. 2010; Paris and Desboeufs 2013). In addition, these results show that sulfur uptake still has the potential to contribute to particle aging, particularly in high-RH environments, although sulfur from SO_2 does not play a role in iron solubility, even at concentrations far above those found in urban atmospheres.

3.6 Acknowledgements

Chapter Four: Advances in single particle inductively coupled plasma mass spectrometry for the analysis of real world samples

4.1 Abstract

An investigation into the formation of Fe particles in seawater led to the discovery of a unique challenge to the measurement of nanoparticles using single particle inductively coupled plasma mass spectrometry (spICPMS). spICPMS is a rapidly growing technique for determining the size of nanoparticles. While spICPMS has been effective in sizing particles in low matrix samples, at least one major knowledge gap remains: identifying a particle in the presence of dissolved analyte. This chapter presents two methods for determining and sizing particles when mixed with dissolved analyte. First, the derivative of the entire data set was used in an attempt to isolate Fe and Au nanoparticle signal from dissolved signal. Second, a novel mathematical approach using the mode and standard deviation of the entire dataset, 100 nm and 60 nm gold (Au) particles were accurately sized when mixed in varying dissolved Au concentrations. These mixed Au samples were also used to determine important parameters for identifying the upper limit of dissolved analyte concentration. These parameters highlighted the importance in considering the standard deviation and not just the ratio of pulse intensities. As an application and demonstration of this method, a nanotechnology-enabled consumer spray containing both dissolved and particulate silver (Ag) was analyzed; the determined Ag particle size matched well with that determined by

transmission electron microscopy. The development of this method will allow for spICPMS to be applied to matrices containing nano-sized particles in the presence of varying concentrations of dissolved analyte, including seawater and freshwater systems, acid mine drainage, and other environmental applications.

4.2 Introduction

4.2.1 Fe in Seawater

Iron solubility in atmospheric PM has been studied at length and on a global scale (Cwiertny et al. 2008; Mahowald et al. 2009; Sholkovitz et al. 2012). The deposition of atmospheric Fe into the ocean is important as Fe is known to be a limiting micronutrient to phytoplankton in remote regions of the ocean (Boyd et al. 2007). However, the concentration of dissolved Fe in seawater only ranges from 0.5-2.0 nM and 50-60% of that has been shown to be colloidal Fe (Wu et al. 2001; Bergquist et al. 2007; Sholkovitz et al. 2012). In seawater Fe usually precipitates as $Fe(OH)_3$ [iron(oxy)hydroxide] (Stumm and Morgan 1996), however colloidal Fe has been shown to contain significant levels of Fe(II) (von der Heyden et al. 2012) a more soluble form of Fe (Majestic et al. 2006; Majestic et al. 2007a). This suggests that there could be an increase in Fe that is more bioavailable and therefore highlights the importance of studying the behavior of atmospherically-deposited Fe in seawater.

Seawater poses a unique challenge for ICP-MS measurements as it contains a high level of total dissolved solids (TDS) leading to a high sample matrix. TDS limits for ICP-MS analysis is typically less than 0.2% (2000 ppm) in order to avoid loss of sensitivity due to matrix deposition on instrument components (McCurdy and Potter

2001). Seawater however, ranges from 35,000-45,000 ppm TDS (Tiwari et al. 2003) posing a problem for the analysis of seawater samples. Diluting the sample would lower the TDS however, this also dilutes any analyte in the sample. For the analysis of trace species in seawater a new way of introducing the sample to the instrument is required.

In the first part of this study, iron sulfates were added to natural seawater to study particle formation. Due to the high sample matrix of the seawater a new method of introducing the sample to the ICP-MS plasma had to be developed. These preliminary studies provided interesting results regarding the formation of iron particles in seawater and yielded another challenge: how to determine a particle signal from that of a dissolved analyte background in single particle inductively coupled plasma mass spectrometry.

4.2.2 spICPMS and the Dissolved Analyte Conundrum

Single particle inductively coupled plasma mass spectrometry (spICPMS) has become a transformative technique for determining the size of nanoparticles in aqueous suspensions (Laborda et al. 2014). In spICPMS, the size of an individual particle is determined based on the intensity of the pulse over the background signal (Pace et al. 2011). spICPMS has been validated against other bulk (dynamic light scattering) and single particle sizing (e.g. SEM and TEM) techniques, also allowing for elemental specificity and higher sample throughput (Montano et al. 2014).

While spICPMS is a powerful tool for sizing nanoparticles, current spICPMS sizing theory requires that the sample baseline is the same as that of the blank (Degueldre et al. 2006; Gschwind et al. 2011; Pace et al. 2011; Mitrano et al. 2012; Pace et al. 2012),

limiting its applicability to systems where the samples have the same baseline as the blank. This is necessary because a particle is determined when the signal intensity is greater than the blank average plus three (or five) times the blank standard deviation (Degueldre et al. 2006). To expand the use of spICPMS to more typical environmental samples, where sample baselines vary as a result of the presence of dissolved analyte and are unpredictable, methods to size particles independent of a laboratory blank need to be developed. A number of studies have suggested different strategies to differentiate a particle from a dissolved analyte background, including 1) removal of dissolved analyte by either chemically pretreating the sample or by coupling a separation technique (Hadioui et al. 2014; Hadioui et al. 2015), 2) decreasing the dwell times (Hineman and Stephan 2014; Montano et al. 2014), or 3) application of post data collection mathematical methods for signal differentiation (Cornelis and Hassellov 2014). However, all of these approaches have potential drawbacks.

Dissolved analyte ions could be removed by coupling spICPMS with chromatographic techniques. Ion exchange columns, micellar electrokinetic chromatography, and complexing agents have all been used in conjunction with spICPMS to remove dissolved analyte ions in the presence of corresponding metallic nanoparticles as well as other major ions (Franze and Engelhard 2014; Hadioui et al. 2014; Hadioui et al. 2015). While these methods have had some success in sizing nanoparticles (Franze and Engelhard 2014; Hadioui et al. 2014; Hadioui et al. 2015), it is possible that changing the sample matrix prior to analysis will shift the equilibrium, possibly affecting the particle size and composition relative to the original composition.

In addition, separation techniques require added complexity and instrumentation which may not be readily available in all laboratory settings.

It has been shown that using microsecond (as opposed to millisecond) dwell times also decreases the background signal (Hineman and Stephan 2014; Liu et al. 2014; Montano et al. 2014; Strenge and Engelhard 2015). In this case, a decreased dwell time, coupled with a constant particle signal, improves the signal-to-noise ratio. While this has great potential, being a more infant technology, it requires updated software and technology (Hineman and Stephan 2014; Liu et al. 2014; Montano et al. 2014; Strenge and Engelhard 2015), again limiting the broad use of this technique. To the best of my knowledge, at this time a more universal method for particle sizing using microsecond dwell times has not been developed.

Finally, mathematical manipulation (post-data collection processing) can be used to identify particles in samples with varying background. One study used a mixed Polyagaussian probability mass function to discriminate between background and nanoparticles (Cornelis and Hassellov 2014). Although this study had success, it was mostly applicable to very small particles (10-15 nm) or samples with high dissolved ion concentration.

The present study offers a much simpler and more broadly applicable mathematical alternative for identifying and sizing particles in samples with varying dissolved analyte, i.e., varying background. The method requires neither instrumental upgrades nor sample preconcentration or separation, and thus it is intended to be applicable to a wide spectrum of researchers. It is demonstrates that, in spICPMS, the

mode of the entire dataset can be used as an alternative of the average blank baseline and that standard deviation of the baseline is easily accessible using the entire dataset. Taking the mode and standard deviation of the dataset as opposed to using the average blank baseline allows for easy discrimination between dissolved and particle analyte. In the presence of dissolved analyte, if the blank average is used, then each dwell time would be erroneously counted as a particle. The method presented in this chapter is used to successfully count and size gold (Au) nanoparticles of known diameter in the presence of dissolved Au up to 50 ppb. The application of this method is demonstrated by using it to size silver (Ag) particles in a nanotechnology-enabled consumer spray containing both dissolved and particle Ag.

4.3 Materials and Methods

4.3.1 Iron Particle Formation in Seawater

To measure the formation of iron particles in seawater, seawater was collected off Ke'e Beach on the north shore of Kauai, Hawaii, USA. Solutions of iron (II) sulfate ($FeSO_4$) and iron(III) sulfate [$Fe_2(SO_4)_3$] were prepared. These solutions were then spiked into the collected seawater at final Fe concentration of 2 nM. Samples were sonicated and for five minutes to prevent particle aggregation and then analyzed via ICP-MS (Agilent 7700). Samples were reanalyzed every five days for 30 days to measure particle formation in seawater.

4.3.2 Adaptation of Sample Introduction System for High Matrix Samples

In order to analyze samples in seawater, the method for sample introduction into the ICP-MS had to be modified. Figure 4.1 shows a schematic for the change in sample

introduction. To dilute the TDS in seawater, samples were introduced via a smaller diameter tube typically used for internal standard introduction. The large diameter tube used for sample introduction allowed deionized water to mix with the seawater sample and dilute the TDS to a reasonable level for ICP-MS analysis while at the same time maintaining particle integrity.

4.3.3 Preparation of gold standards and samples

Gold (Au) particles were determined over the background and sized using established methods for spICPMS.(Pace et al. 2011; Montano et al. 2014) Au nanoparticles (100 nm diameter, BBI Solutions, Cardiff, Wales, UK) were used to determine the transport efficiency, a necessary variable for determining the size of unknown nanoparticles. To develop a method for differentiating a particle signal from that of dissolved analyte, 60 and 100 nm Au nanoparticles (BBI Solutions) and a dissolved Au standard (High Purity Standards, Charleston, SC, USA) were used to prepare mixed nanoparticle and dissolved analyte samples. Au nanoparticle suspensions were combined with varying dissolved Au concentrations (0.0, 0.5, 1.0, 2.0, 5.0, 10.0, 15.0, 20.0, and 50.0 ppb) for the spICPMS analysis. To reduce the possibility of coincidence, Au nanoparticles were spiked into a final concentration of 50 ppt (parts per trillion) for 100 nm Au particles and 10 ppt for 60 nm Au particles (smaller particles leads to a higher particle concentration in solution). All samples were acidified to 2% HCl, which was found did not have any effect on the particle size and number. Samples were analyzed using a quadrupole ICP-MS (Agilent 7700) operating with 10 ms dwell times and a sample analysis time of 200 s, for a total collection of ~20,000 dwell times.
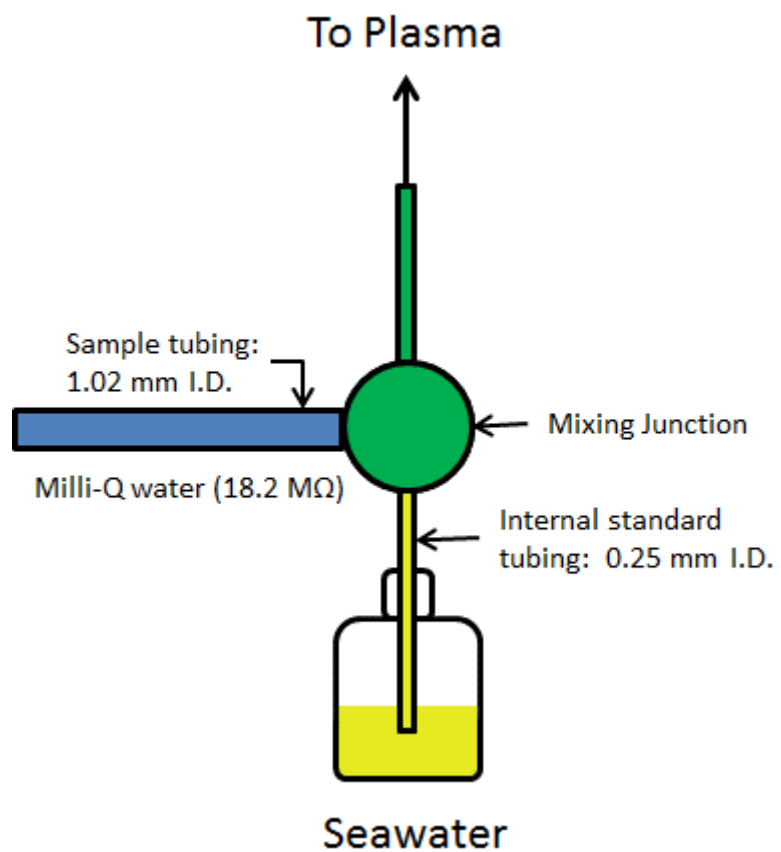
Figure 4.1: Schematic of the changes made to the ICP-MS sample introduction system to account for the high matrix of seawater.

4.3.4 Data analysis and method development

The first approach was to calculate the derivative for each data point. A "cut-off" derivative value was determined and anything above that value was deemed a particle and removed from the dataset. Once particles were removed the remaining data points were averaged to calculate a baseline unique to that sample. Again the average plus 3σ was used to determine a nanoparticle. The second method reported in this study takes advantage of the fact that, in spICPMS, only ~1% of the dwell times result in a particle "hit." Therefore, ~99% of the measurements are that of the baseline, which includes isobaric interferences, as well as dissolved analyte. Since almost all integrations are of the baseline, the mode of the dataset will actually be the average of the baseline. The mode is easily acquired and is used as the sample-specific baseline intensity. Additionally, the standard deviation of the entire dataset is determined from a regression analysis using a statistical software package (SigmaPlot 12.0). Again, this is a result of the fact that 99% of the measurements in spICPMS are of baseline. Then, using the mode of the sample set, a threshold value was determined using the mode plus 5σ. All signal intensities above this threshold are considered particles and these were sized according to standard spICPMS theory (Pace et al. 2011), but with sample-specific backgrounds. In the presence of varying dissolved analyte, the mode works as a better measurement than the average because the mode is essentially the average of the background and most of the data collected in spICPMS is background signal. The mean, however, would provide an average of the background and particle signals thus not being a true representation of the actual background.

4.3.5 Nanotechnology-enabled consumer spray

As an application and demonstration of the method reported herein, a nanotechnology-enabled consumer spray described by its manufacturer as containing silver nanoparticles was investigated and both Ag nanoparticles and dissolved Ag were found using spICPMS. To validate the method above, the Ag spray sample was also analyzed using transmission electron microscopy (TEM). For TEM, Ag particles were separated from the dissolved Ag in the nanospray by centrifugation at ~17,000 x g for 1 hr (Eppendorf Centrifuge 5418) and the resulting pellet was washed with high purity water (18.2 MΩ-cm), resuspended, and spun down again. This process was repeated three times. After the final washing, particles were resuspended and deposited on to a copper-coated TEM grid. A scanning TEM (Philips CM 200) was used to measure Ag particle size.

4.4 Results

4.4.1 Derivative Method for Determination of Fe Particles in Seawater

Figure 4.2 shows the time resolved spectrum for $Fe_2(SO_4)_3$ dissolved in seawater. Intense peaks in signal can be observed indicating the presence of Fe particles in the seawater. The inset text shows the average, standard deviation (σ), and the nanoparticle count. In the two sets of text there is a noticeable difference in these values. In the standard method, a particle is determined by taking the average of the blank plus 3σ of the blank. If a signal pulse is greater than that it is considered to be a particle.
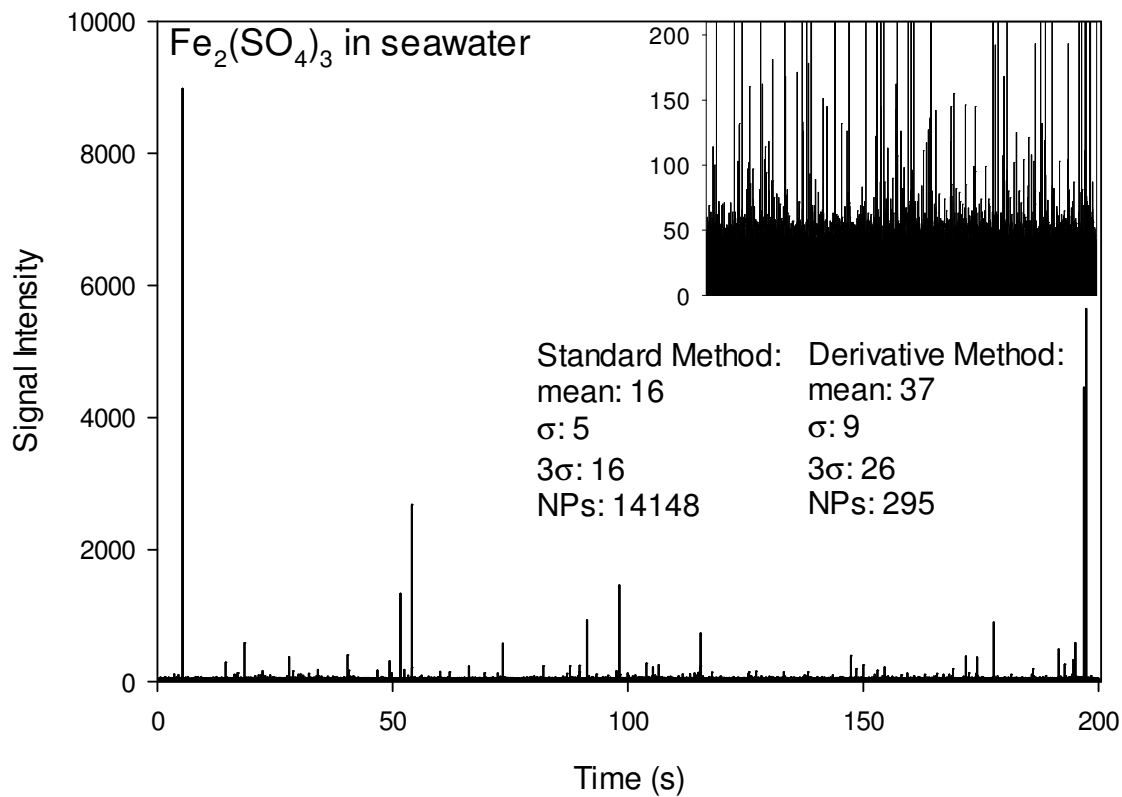
Figure 4.2: Raw spICPMS data of $Fe_2(SO_4)_3$ in seawater. Text shows the baseline data as a comparison of two different methods of analysis. The insert provides an enhanced view of the baseline for the entire dataset.
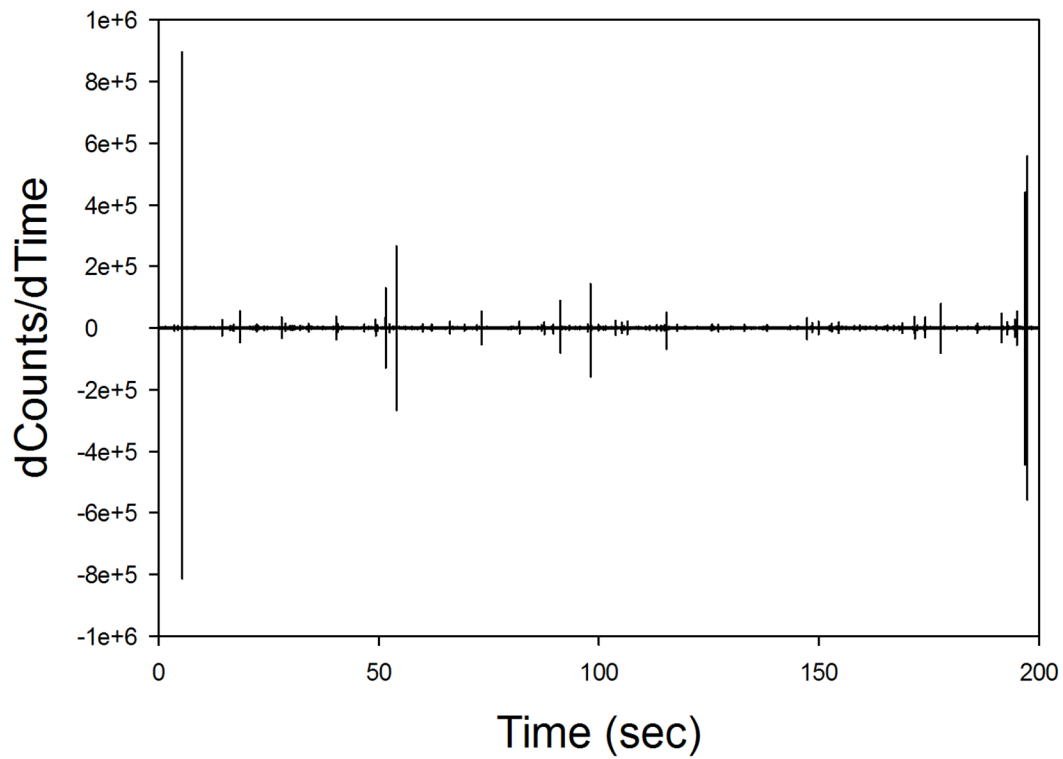
Figure 4.3: First derivative plot of $Fe_2(SO_4)_3$ in seawater (Figure 4.2). Intense pulses represent particle pulses.

In the derivative method, the derivative of the entire data set is acquired (shown in

Figure 4.3) and a cut-off value determined. The cut-off value allows for the identification

and subsequent removal of particles from the dataset. Once particles have been removed

from the dataset a baseline unique to that sample can be determined to account for

dissolved analyte (Fe in this case). When accounting for the dissolved Fe, the average

and standard deviation of the baseline increases leading to a decrease in the particle

count. As can be seen in the insert in Figure 4.2, the signal intensity of the baseline is

around 100 counts. In the standard method the baseline of the blank is almost half of that

of the baseline determined by the derivative method. As a result, signal pulses

representing dissolved analyte (the cause for the increased baseline above that of the

blank) were being counted as particles hence the large discrepancy in nanoparticle count.

Using this method, particle counts were determined for a month for $Fe_2(SO_4)_3$ and $FeSO_4$

in seawater.

As can be seen in Figure 4.4, particle counts increased over the month for

$Fe_2(SO_4)_3$ while particle counts remained the same for $FeSO_4$. The obvious outlier would

be the decrease in counts in the last data point for the $Fe_2(SO_4)_3$. While this method was

initially successful in isolating particle signal, it broke down at dissolved analyte

concentrations lower than the second method. Also, the cut-off value was completely

arbitrary with no real statistical support. This led to the development of the second

method.
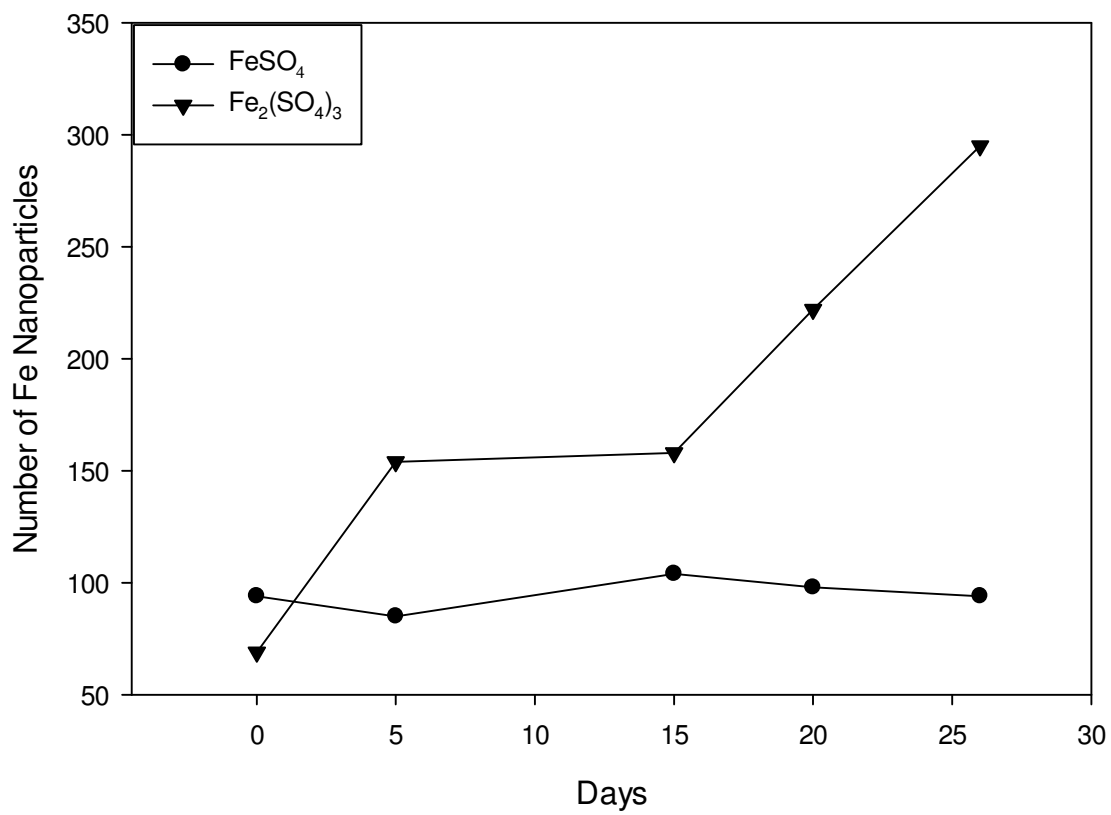
Figure 4.4: Nanoparticle counts over time for FeSO$_4$ (circles) Fe$_2$(SO$_4$)$_3$ (triangles).

4.4.2 Mathematical Method for Determining Particles in the Presence of Dissolved Analyte

Figures 4.5-4.8 show 100 nm and 60 nm Au particles mixed with varying concentrations of dissolved Au, while mean sizes of the observed size distributions are presented in Table 4.1. Figure 4.5 shows the results of 100 nm particles with no dissolved Au and sized by standard techniques using the blank baseline. By comparison, Figure 4.6 utilizes the method presented, showing 100 nm Au particles mixed with 1.0 ppb dissolved Au. In Figure 4.6, 100 nm particles were accurately sized (Figure 4.6C) using the mode and standard deviation of the dataset. 60 nm Au particles mixed with 1.0 ppb dissolved Au (Figure 4.7) were used to test the robustness of the method and were accurately sized. Figure 4.8 shows 60 nm Au particles in 5.0 ppb dissolved Au. As can be seen in Figure 4.8B, the lower end of the particle fraction is contained within the upper end of the dissolved fraction of the sample, ultimately resulting in an increased measured particle size (67 nm). The baseline distribution in Figure 4.8 is much larger than in Figure 4.7 which suggests that the standard deviation of the baseline, used in particle determination, has a significant impact on the limits of the method.

Table 4.1 presents measured size distribution parameters for 60 and 100 nm Au particles at different dissolved Au concentrations, including those presented in Figures 4.5-4.8. Average particle size and uncertainty (expressed as the geometric mean and geometric standard deviation) (Hinds 1999), the standard deviation of the entire dataset, the standard deviation of only the baseline, the ratio of the average particle pulse to
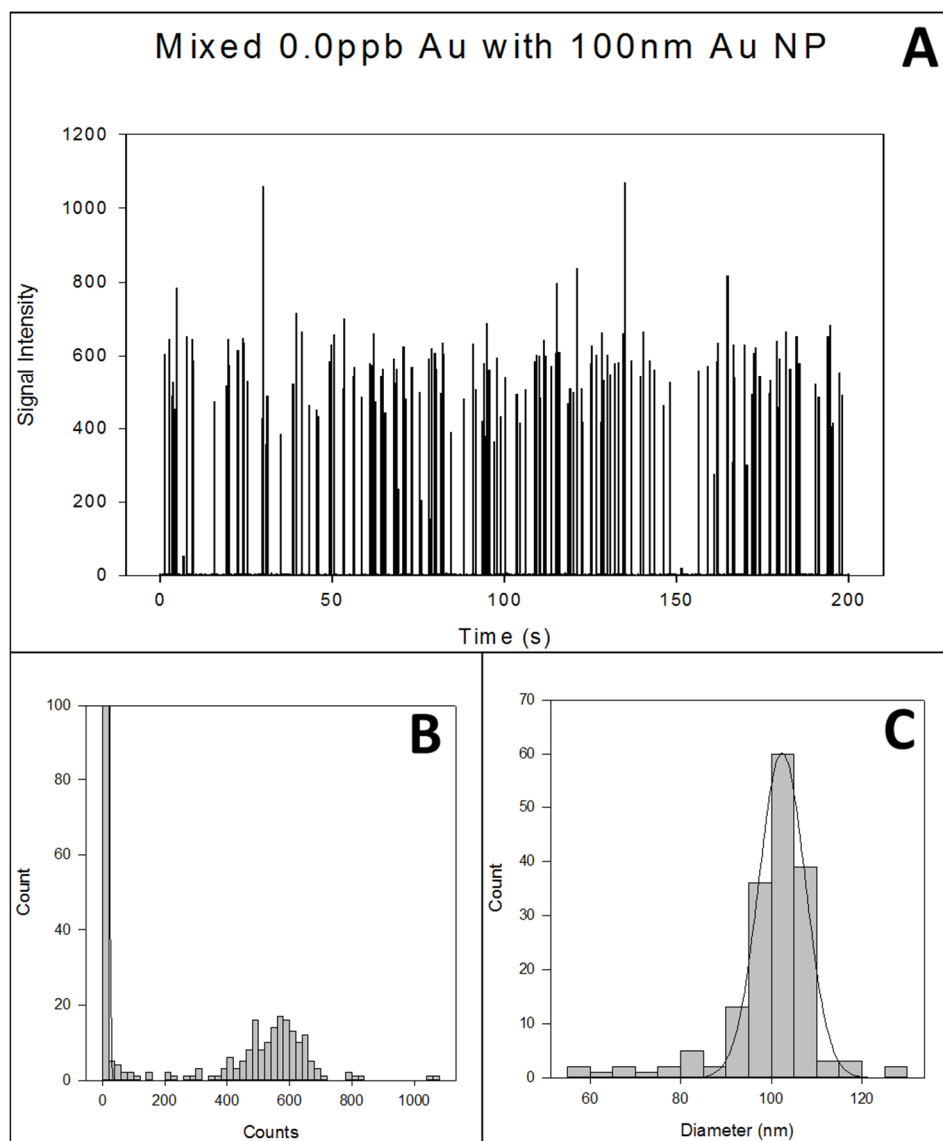
Figure 4.5: Data processing of 100 nm Au nanoparticles in MilliQ (18.2 MΩ-cm). A) Raw data from spICPMS B) Distribution of raw data C) Size distribution of particles.
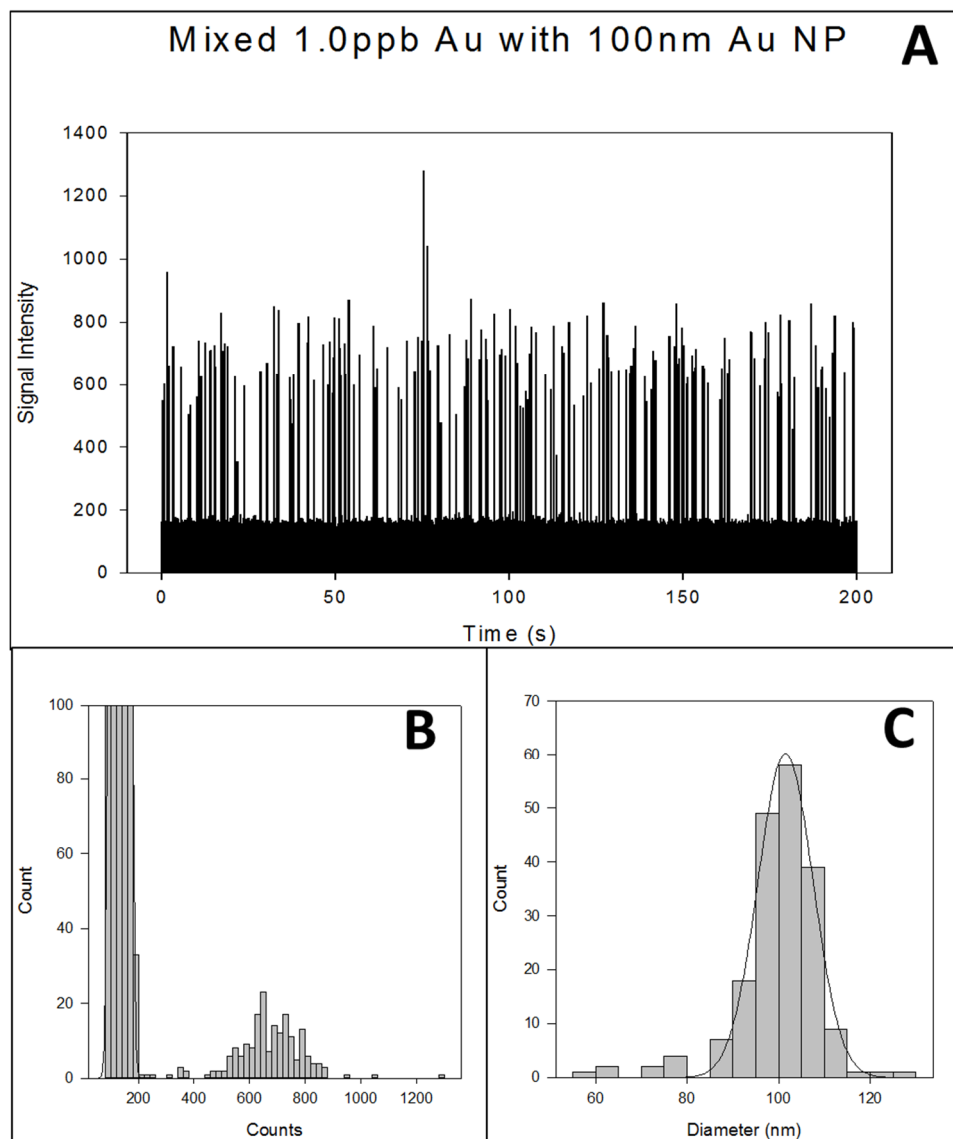
Figure 4.6: Data processing of 100 nm Au nanoparticles mixed with 1.0 ppb dissolved Au. A) Raw data from spICPMS B) Distribution of raw data C) Size distribution of particles.
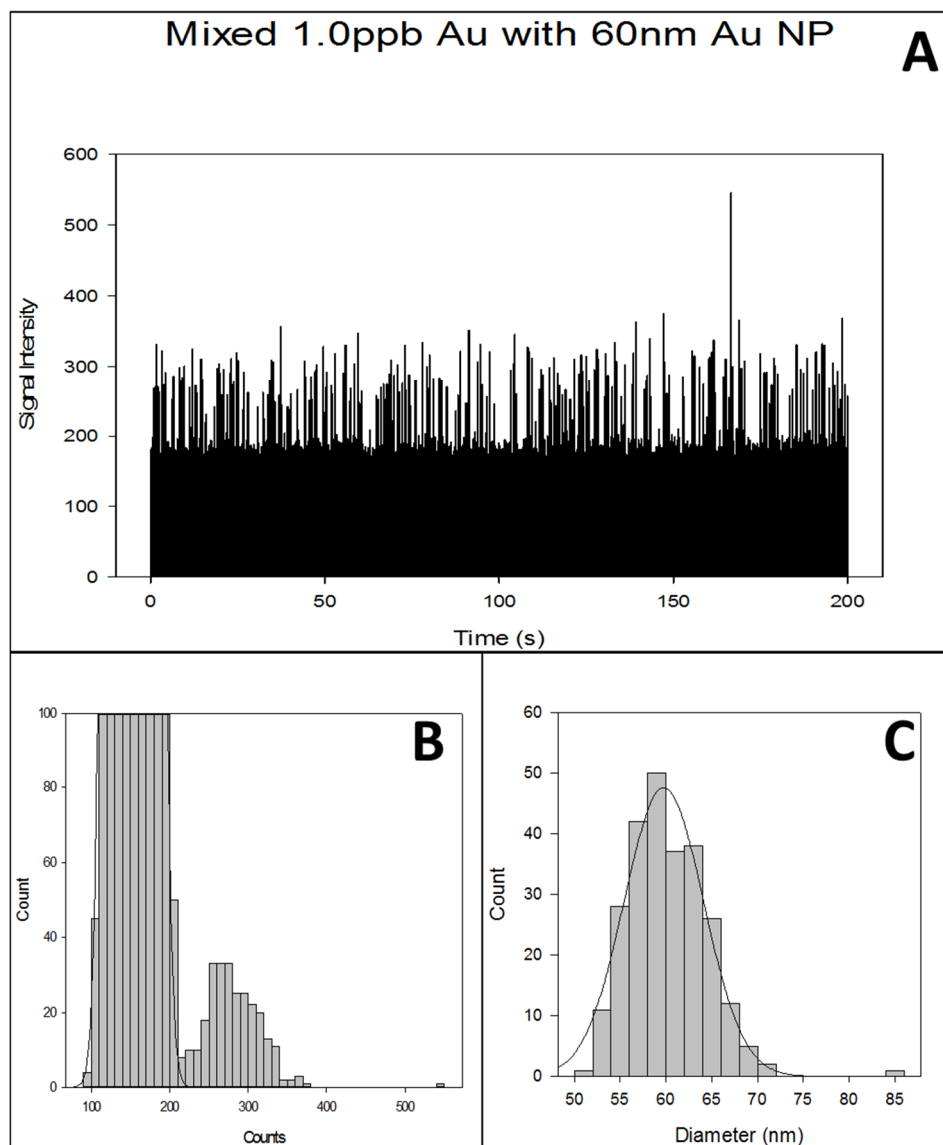
Figure 4.7: Data processing of 60 nm Au nanoparticles mixed with 1.0 ppb dissolved Au. A) Raw data from spICPMS B) Distribution of raw data C) Size distribution of particles.
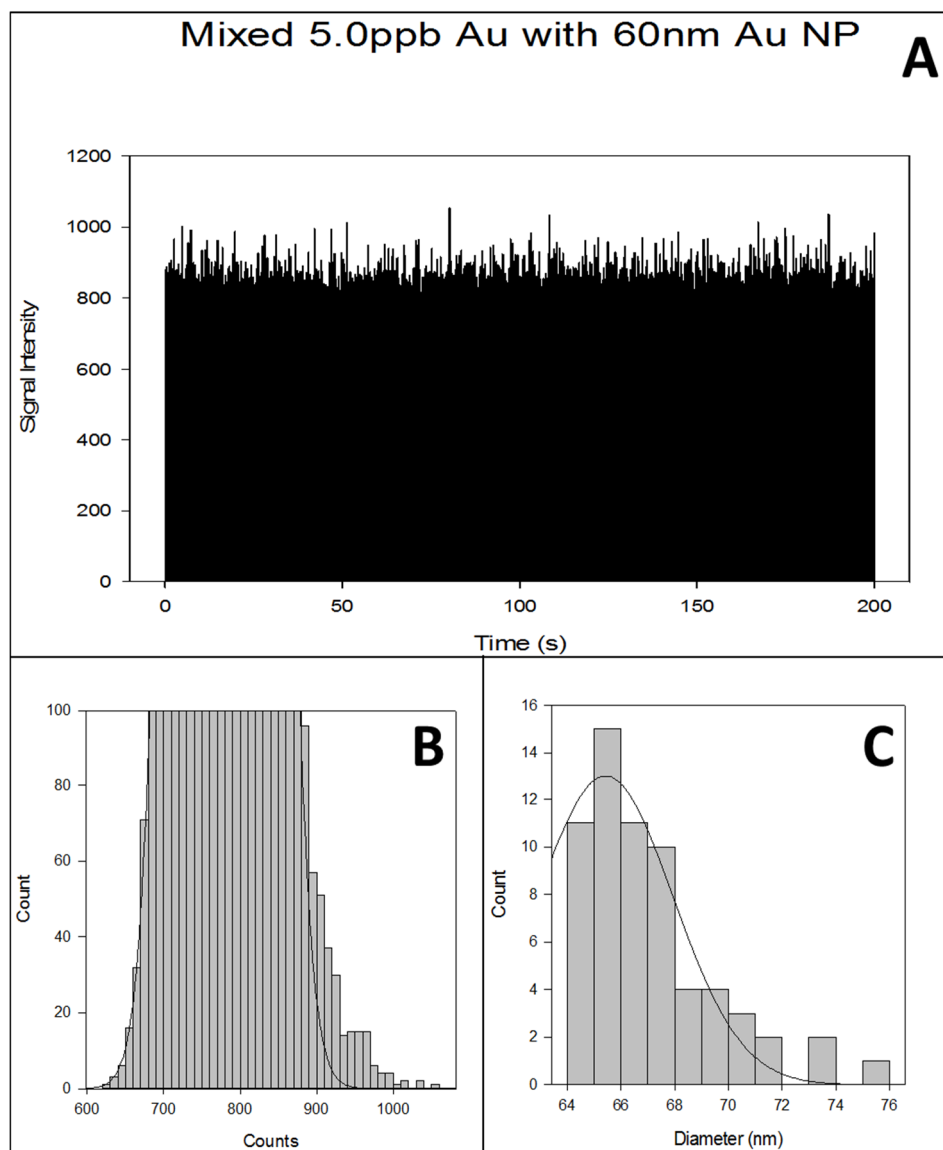
Figure 4.8: Data processing of 60 nm Au nanoparticles mixed with 5.0 ppb dissolved Au. A) Raw data from spICPMS B) Distribution of raw data C) Size distribution of particles.

Table 4.1: Parameters used for method development for all mixed samples. Average particle size and uncertainty reported as geometric mean (d_g) and geometric standard deviation (σ_g) respectively.

Dissolve Au Concentration (ppb)	Average Particle Size (nm, $d_g \pm \sigma_g$)	Particle Count	σ_{raw}	$\sigma_{baseline}$	Average Particle Pulse / Baseline Pulse	$\sigma_{baseline}$ / Particle Pulse
100 nm						
0.0	100 ± 1	171	16.4	2.34*	536	0.004
0.5	100 ± 1	188	8.48	5.61	9.19	0.010
1.0	100 ± 1	192	9.11	8.73	3.98	0.016
2.0	95 ± 1	155	13.6	12.3	1.91	0.025
5.0	101 ± 1	182	21.4	20.5	0.90	0.037
10.0	101 ± 1	182	56.5	54.6	0.40	0.099
15.0	95 ± 1	195	55.7	55.5	0.31	0.122
20.0	98 ± 1	165	72.3	71.5	0.26	0.146
50.0	110 ± 1	16	131	129	0.15	0.185
60 nm						
0.0	60 ± 1	246	7.17	6.93	72.8	0.054
0.5	59 ± 1	258	10.1	10.1	1.89	0.082
1.0	60 ± 1	253	16.1	15.9	0.86	0.121
2.0	62 ± 1	152	23.6	23.4	0.48	0.158
5.0	67 ± 1	63	40.4	40.4	0.28	0.172

* indicates statistical differences ($p < 0.05$) between σ_{raw} and $\sigma_{baseline}$ ($N = 3$).

background pulse, the ratio of the baseline standard deviation ($\sigma_{baseline}$) to the average particle pulse, and the number of particles counted for each sample are shown. First, Table 4.1 shows that the standard deviation determined for the entire dataset is statistically similar ($p > 0.05$) to the standard deviation of the baseline when dissolved analyte is present, with the exception of the 100 nm particles mixed with no Au. Further, as highlighted in Table 4.1, 100 nm particles were accurately sized and counted up to 20 ppb dissolved Au. The cutoff is recognized as a decrease in number of particles as well as an increase in mean particle size. Conversely, 60 nm Au particles could only be accurately sized up to 2.0 ppb dissolved Au.

Given the large differences in acceptable dissolved concentrations, we inspected which parameters affect the upper dissolved concentration limit in which a particle could be sized. At a $\sigma_{baseline}$/particle of about 0.13-0.14, we observe a decrease in particle count and an increase in particle size for both particle sizes, indicating that the particle pulse needs to be 7.5-8 times that of the baseline noise. Conversely, the particle pulse-to-baseline pulse ratio breaks down at different values for 100 nm (0.26) versus 60 nm (0.48), indicating that pulse intensity is not a reliable metric of the ability to identify particles. These parameters shown in Table 4.1 highlight the importance of considering the standard deviation-to-pulse ratio and not just the particle pulse-to-baseline pulse ratio. The major result here is that the particle intensity adds on top of the baseline to a point at which the noise of the baseline ($\sigma_{baseline}$) becomes too great to accurately identify particles because it overtakes the smaller part of the distribution.

73

Figure 4.9 presents an application of the method above; applying it to a nanotechnology-enabled consumer spray containing both dissolved and particle Ag. Here, the raw data, size distribution, and TEM of the sample are shown. The results from the spICPMS analysis (Figure 4.9B, mean diameter presented as geometric mean and geometric standard deviation) matched well with the TEM measurements (Figure 4.9C). In both it can be seen that the average particle diameter is approximately 30 nm. Conversely, if these particles were sized using standard spICPMS methods (average blank baseline), then pulses representing dissolved Ag would be counted as particles, leading to a decrease in particle size (21.5 ± 8.8 nm) and an increase in particle count from 132 to 6612 particles (1% versus 33% of the dwell times).

In this study, it is reported that using the mode plus 5σ was successful in discriminating between dissolved and particle Au and Ag. An upper dissolved concentration limit was determined for 100 nm (above 20 ppb) and 60 nm (above 2 ppb) Au particles, indicated by a $\sigma_{baseline}$/particle pulse ratio 0.13-0.14. At ratios above 0.13, the lower portion of the size distribution becomes lost in the baseline noise. The method was then demonstrated and validated using a nanotechnology-enabled consumer spray containing particle and dissolved Ag, where the particle size was determined with spICPMS and verified with TEM. Also, the use of traditional baseline methods results in erroneous particle size and number calculations, whereas the application of the method presented here is able to account for dissolved baseline as shown by the results from the nanotechnology-enabled consumer spray. Finally, this method will allow for a broader
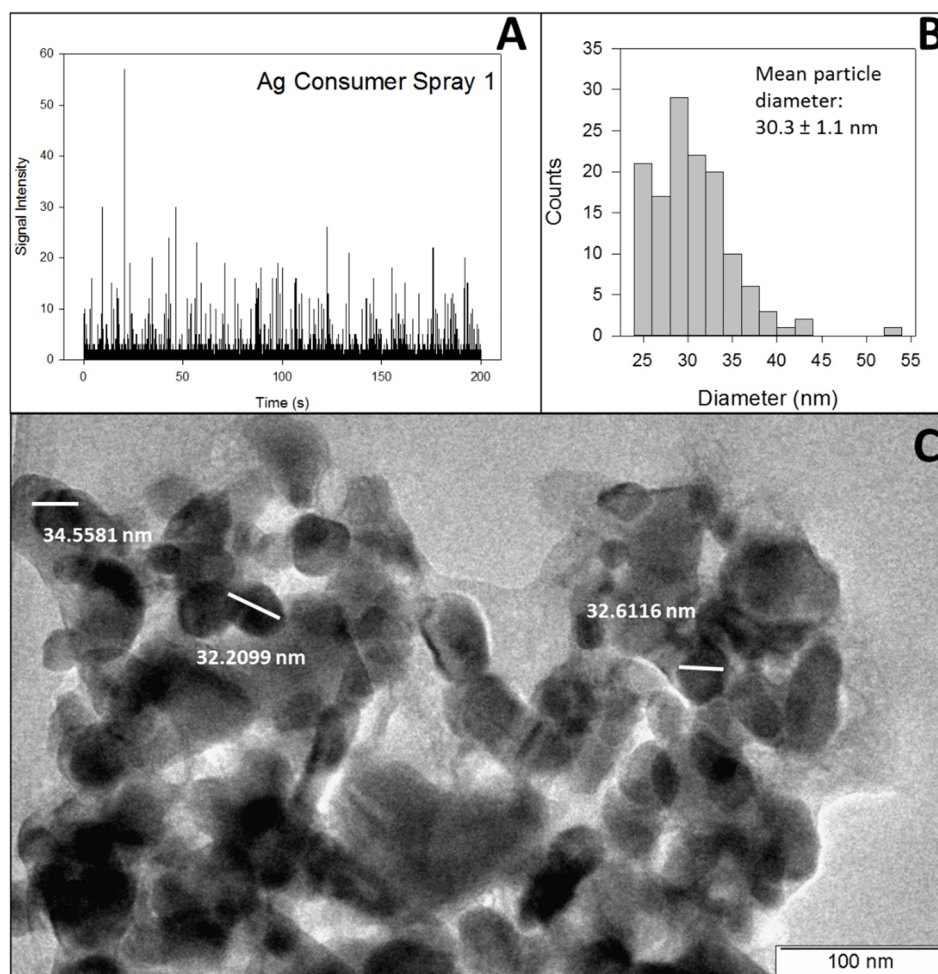
Figure 4.9: Application of the method to an Ag containing nanotechnology-enabled consumer spray. A) Raw spICPMS data. B) Size distribution of Ag particles determined from spICPMS. C) TEM of the nanotechnology-enabled consumer spray.

application of spICPMS on environmental samples containing both dissolved and particle analyte such as acid mine drainage (Carbone et al. 2005; Seo et al. 2010), iron in seawater (Sholkovitz et al. 2012), and other applications, including consumer nanotechnology products, without the need to first remove dissolved analyte or invest in instrumentation upgrades.

4.5 Acknowledgements

Chapter Five: Summary and Future Work

The major driving force behind this work was to gain further understanding of how Fe solubility changes through atmospheric transport and deposition and chemical and physical interactions with surrounding metals and other atmospheric species. Since Fe is the most common transition metal in the Earth's crust and in atmospheric PM and due to the potential for oxidation and reduction, the changes in Fe solubility can have a great effect on both the environment and human health. However, through the drive to further understand the behavior of Fe in environmental matrices, other metals could be and were studied as these other metals too can pose health and ecological risks while providing important information about the source of a sample.

In the study presented in Chapter 2, the effects of a completely ground-level light rail system on the metal concentrations in ambient PM were measured. The overwhelming majority of studies relating to metals from rail-based transportation systems focused on underground subway systems with very few considering ground-level rail systems. Through the collection of samples on board and next to the trains, as well as at an urban background location, it was seen that metal concentrations were highest (on a per mass basis) in the samples collected on board the train. This study also contributed to the growing dataset of metal concentrations in PM in the region. Another important finding in this study is that the Fe solubility in the $PM_{2.5}$ collected was around 20% with typical Fe solubility being 2% or less. This is a result of the contribution of

anthropogenic iron from sources such as combustion to the total Fe in the PM. Fe

solubilization continues to be a topic of interest and studying combustion Fe is the basis

for ongoing projects in the laboratory. The potential for further work with this project

lies with expanding the sample collection to determine an emission rate of metals by the

light rail. This could lead to a better understanding of the impact of the light rail on the

metals budget in regional PM especially when compared to an emission rate for

automobile traffic.

Chapter 3 focused exclusively on Fe and Fe solubilization through atmospheric

transport. Though numerous previous studies important variables such as particle size,

source of Fe (anthropogenic, natural, or both), and interaction with other atmospheric

species (SO_2), most have made these observations using collected PM, a complex matrix.

Through the use of lab-created simulated marine particles, each variable could be

independently studied to isolate the most important variable affecting Fe solubilization.

It was determined, through the exposure of different Fe samples, that particle size and

mineralogy of Fe-containing particles had the greatest effects on changing Fe solubility,

while relative humidity and exposure to SO_2 had no noticeable effects. It was observed

through SEM-EDS that the particles did uptake sulfur however this did not affect the Fe

chemistry as highlighted by XANES measurements.

The importance of determining the variables affecting Fe solubilization is vast.

So many studies have used models and measurements to predict and understand the

source of the Fe in PM and subsequent transport and deposition in attempts to explain Fe

solubilization across the globe. With the elucidation of these variables it is possible that

these models could be updated to account for variables such as particle size. The particle size variable is of extra interest because anthropogenic combustion particles are typically smaller and containing more soluble Fe. Accounting for these variables could increase our understanding of more soluble Fe and potential bioavailability. The source of combustion Fe is continuing to drive research in the laboratory where a current graduate student is studying automobile exhaust as a source of combustion Fe.

The potential bioavailability of Fe in the ocean provided the motive for the exploration of Fe particle formation in seawater (Chapter 4). Through the addition of iron sulfates to natural seawater, Fe particles were observed to form over time through spICPMS measurements. This initial exploration of Fe particles in seawater yielded two unique challenges: 1) adaptation of the ICP-MS sample introduction system to account for the high sample matrix of the seawater (high TDS) and 2) a need for a new treatment of spICPMS data to account for dissolved analyte increasing the baseline above that of a normal blank sample. The first challenge was resolved by rearranging the existing sample introduction system to dilute the sample while not disrupting the Fe particles. The second challenge was not as readily resolved and two approaches were explored.

The two methods for addressing dissolved analyte in spICPMS data were both centered on the mathematical treatment of the data so that added/upgraded instrumentation could be avoided. The first method was to take the derivative of the entire dataset to selectively isolate and remove particle pulses from the dataset to calculate a baseline unique to each sample. While this method was successful, it was also arbitrary, as a "cut-off" value had to be selected in order to distinguish a particle pulse

from that of the baseline. As a result an approach with more of a statistical basis was desired.

The second approach used the standard deviation and the mode of the entire dataset. The mode was found to be a better representation of the baseline than the mean as 99% of the spICPMS data is baseline making the mode the average of the baseline. Using well characterized Au particles, this method was tested and several statistical parameters were developed. This method yielded a much more robust way for separating a particle pulse from an increased baseline due to dissolved analyte. This method also highlighted the importance of considering the standard deviation-to-pulse ratio and not just the particle pulse-to-background pulse ratio. This method was then validated using a nanotechnology-enabled consumer spray containing both particle and dissolved Ag. The successful development of a mathematical method improves the applicability of spICPMS to many more environmental samples and matrices. This method also allows for a more universal use of spICPMS because added instrumentation or upgraded software to account for the dissolved analyte is not required. Finally, with this method, work can return to studying Fe particles in seawater.

Through the measurement of metals in environmental matrices, this work has been able to contribute to a growing dataset about regional air quality, elucidated important variables regarding Fe solubility in atmospheric PM, and improved the applicability of spICPMS to environmental samples. It is my hope that by filling these knowledge gaps, future researchers can expand on these topics and continue to add to the knowledge of the chemistry of particle-bound metals in environmental samples

References

Aarnio, P., T. Yli-Tuomi, et al. (2005). "The concentrations and composition of and exposure to fine particles (PM2.5) in the Helsinki subway system." Atmospheric Environment **39**(28): 5059-5066.

Adams, H. S., M. J. Nieuwenhuijsen, et al. (2001). "Fine particle (PM2.5) personal exposure levels in transport microenvironments, London, UK." Science of the Total Environment **279**(1-3): 29-44.

Aguilar-Islas, A. M., J. F. Wu, et al. (2010). "Dissolution of aerosol-derived iron in seawater: Leach solution chemistry, aerosol type, and colloidal iron fraction." Marine Chemistry **120**(1-4): 25-33.

Baker, A. R. and P. L. Croot (2010). "Atmospheric and marine controls on aerosol iron solubility in seawater." Marine Chemistry **120**(1–4): 4-13.

Baker, A. R. and T. D. Jickells (2006). "Mineral particle size as a control on aerosol iron solubility." Geophysical Research Letters **33**(17).

Baltrusaitis, J., D. M. Cwiertny, et al. (2007). "Adsorption of sulfur dioxide on hematite and goethite particle surfaces." Physical Chemistry Chemical Physics **9**(41): 5542-5554.

Benoit, G., S. D. Oktaymarshall, et al. (1994). "Partitioning of Cu, Pb, Ag, Zn, Fe, Al, and Mn between filter-retained particles, colloids, and solution in six Texas estuaries." Marine Chemistry **45**(4): 307-336.

Bergquist, B. A., J. Wu, et al. (2007). "Variability in oceanic dissolved iron is dominated by the colloidal fraction." Geochimica Et Cosmochimica Acta **71**(12): 2960-2974.

Bowie, A. R., D. Lannuzel, et al. (2009). "Biogeochemical iron budgets of the Southern Ocean south of Australia: Decoupling of iron and nutrient cycles in the subantarctic zone by the summertime supply." Global Biogeochemical Cycles **23**(4): GB4034.

Boyd, P. W., T. Jickells, et al. (2007). "Mesoscale iron enrichment experiments 1993-2005: Synthesis and future directions." Science **315**(5812): 612-617.

Buck, C. S., W. M. Landing, et al. (2010a). "Particle size and aerosol iron solubility: A high-resolution analysis of Atlantic aerosols." Marine Chemistry **120**(1-4): 14-24.

Buck, C. S., W. M. Landing, et al. (2010b). "The solubility and deposition of aerosol Fe and other trace elements in the North Atlantic Ocean: Observations from the A16N CLIVAR/CO2 repeat hydrography section." Marine Chemistry **120**(1-4): 57-70.

Carbone, C., F. Di Benedetto, et al. (2005). "Natural Fe-oxide and -oxyhydroxide nanoparticles: an EPR and SQUID investigation." Mineralogy and Petrology **85**(1-2): 19-32.

Carvacho, O. F., L. L. Ashbaugh, et al. (2004). "Measurement of PM2.5 emission potential from soil using the UC Davis resuspension test chamber." Geomorphology **59**(1-4): 75-80.

Cass, G. R. and G. J. McRae (1983). "Source-receptor reconciliation of routine air monitoring data for trace metals: an emission inventory assisted approach." Environmental Science & Technology **17**(3): 129-139.

Chan, L. Y., W. L. Lau, et al. (2002). "Commuter exposure to particulate matter in public transportation modes in Hong Kong." Atmospheric Environment **36**(21): 3363-3373.

Chen, H. and V. H. Grassian (2013). "Iron dissolution of dust source materials during simulated acidic processing: the effect of sulfuric, acetic, and oxalic acids." Environmental science & technology **47**(18): 10312-10321.

Chen, Y., J. Street, et al. (2006). "Comparison between pure-water- and seawater-soluble nutrient concentrations of aerosols from the Gulf of Aqaba." Marine Chemistry **101**(1–2): 141-152.

Cheng, K. C., M. D. Goebes, et al. (2010). "Association of size-resolved airborne particles with foot traffic inside a carpeted hallway." Atmospheric Environment **44**(16): 2062-2066.

Cheng, Y. H. and Y. L. Lin (2010). "Measurement of Particle Mass Concentrations and Size Distributions in an Underground Station." Aerosol and Air Quality Research **10**(1): 22-29.

Chester, R. and T. D. Jickells (2012). Marine Geochemistry, Wiley.

Chillrud, S., D. Grass, et al. (2005). "Steel dust in the New York City subway system as a source of manganese, chromium, and iron exposures for transit workers." Journal of Urban Health **82**(1): 33-42.

Chillrud, S. N., D. Epstein, et al. (2003). "Elevated Airborne Exposures of Teenagers to Manganese, Chromium, and Iron from Steel Dust and New York City's Subway System." Environmental Science & Technology **38**(3): 732-737.

Chillrud, S. N., D. Epstein, et al. (2004). "Elevated Airborne Exposures of Teenagers to Manganese, Chromium, and Iron from Steel Dust and New York City's Subway System." Environmental Science & Technology **38**(3): 732-737.

Chin, M., T. Diehl, et al. (2007). "Intercontinental transport of pollution and dust aerosols: implications for regional air quality." Atmospheric Chemistry and Physics **7**(21): 5501-5517.

Chuang, P. Y., R. M. Duvall, et al. (2005). "The origin of water soluble particulate iron in the Asian atmospheric outflow." Geophysical Research Letters **32**(7).

Clements, N., J. Eav, et al. (2014). "Concentrations and source insights for trace elements in fine and coarse particulate matter." Atmospheric Environment **89**: 373-381.

Connell, D. W. (2005). Basic concepts of environmental chemistry. Boca Raton, FL, CRC/Taylor & Francis.

Cornelis, G. and M. Hassellov (2014). "A signal deconvolution method to discriminate smaller nanoparticles in single particle ICP-MS." Journal of Analytical Atomic Spectrometry **29**(1): 134-144.

Cwiertny, D. M., J. Baltrusaitis, et al. (2008). "Characterization and acid-mobilization study of iron-containing mineral dust source materials." Journal of Geophysical Research: Atmospheres **113**(D5): D05202.

Dasch, J. and G. Wolff (1989). "Trace inorganic species in precipitation and their potential use in source apportionment studies." Water, Air, and Soil Pollution **43**(3-4): 401-412.

Deboudt, K., A. Gloter, et al. (2012). "Red-ox speciation and mixing state of iron in individual African dust particles." Journal of Geophysical Research: Atmospheres **117**(D12): D12307.

Degueldre, C., P. Y. Favarger, et al. (2006). "Gold colloid analysis by inductively coupled plasma-mass spectrometry in a single particle mode." Analytica Chimica Acta **555**(2): 263-268.

DiStefano, E., A. Eiguren-Fernandez, et al. (2009). "Determination of metal-based hydroxyl radical generating capacity of ambient and diesel exhaust particles." Inhalation Toxicology **21**(8-11): 731-738.

Dockery, D. W., C. A. Pope, et al. (1993). "An Association between Air Pollution and Mortality in Six U.S. Cities." New England Journal of Medicine **329**(24): 1753-1759.

Duce, R. A., P. S. Liss, et al. (1991). "The Atmospheric Input of Trace Species to the World Ocean." Global Biogeochemical Cycles **5**(3): 193-260.

Duvall, R. M., B. J. Majestic, et al. (2008). "The water-soluble fraction of carbon, sulfur, and crustal elements in Asian aerosols and Asian soils." Atmospheric Environment **42**(23): 5872-5884.

Faiola, C., A. M. Johansen, et al. (2011). "Ultrafine Particulate Ferrous Iron and Anthracene Associations with Mitochondrial Dysfunction." Aerosol Science and Technology **45**(9): 1109-1122.

Falkowski, P. G., R. T. Barber, et al. (1998). "Biogeochemical controls and feedbacks on ocean primary production." Science **281**(5374): 200-206.

Faust, B. C. and M. R. Hoffmann (1986). "Photoinduced reductive dissolution of alpha-Fe_2O_3 by bisulfite." Environmental Science & Technology **20**(9): 943-948.

Field, C. B., M. J. Behrenfeld, et al. (1998). "Primary production of the biosphere: Integrating terrestrial and oceanic components." Science **281**(5374): 237-240.

Finlayson-Pitts, B. J. and J. N. Pitts Jr (2000). Chemistry of the Upper and Lower Atmosphere. San Diego, Academic Press.

Franze, B. and C. Engelhard (2014). "Fast Separation, Characterization, and Speciation of Gold and Silver Nanoparticles and Their Ionic Counterparts with Micellar Electrokinetic Chromatography Coupled to ICP-MS." Analytical Chemistry **86**(12): 5713-5720.

Furuya, K., Y. Kudo, et al. (2001). "Seasonal variation and their characterization of suspended particulate matter in the air of subway stations." Journal of Trace and Microprobe Techniques **19**(4): 469-485.

Gao, Y., S. M. Fan, et al. (2003). "Aeolian iron input to the ocean through precipitation scavenging: A modeling perspective and its implication for natural iron fertilization in the ocean." Journal of Geophysical Research-Atmospheres **108**(D7).

Garg, B. D., S. H. Cadle, et al. (2000). "Brake wear particulate matter emissions." Environmental Science & Technology **34**(21): 4463-4469.

Gerdol, R., L. Bragazza, et al. (2000). "Monitoring of heavy metal deposition in Northern Italy by moss analysis." Environmental Pollution **108**(2): 201-208.

Ghio, A. J., J. Stonehuerner, et al. (1999). "Metals associated with both the water-soluble and insoluble fractions of an ambient air pollution particle catalyze an oxidative stress." Inhalation Toxicology **11**(1): 37-49.

Goldsmith, C. A. W., A. Imrich, et al. (1998). "Analysis of air pollution particulate-mediated oxidant stress in alveolar macrophages." Journal of Toxicology and Environmental Health, Part A: Current Issues **54**(7): 529-545.

Gschwind, S., L. Flamigni, et al. (2011). "Capabilities of inductively coupled plasma mass spectrometry for the detection of nanoparticles carried by monodisperse microdroplets." Journal of Analytical Atomic Spectrometry **26**(6): 1166-1174.

Hadioui, M., V. Merdzan, et al. (2015). "Detection and Characterization of ZnO Nanoparticles in Surface and Waste Waters Using Single Particle ICPMS." Environmental Science & Technology **49**(10): 6141-6148.

Hadioui, M., C. Peyrot, et al. (2014). "Improvements to Single Particle ICPMS by the Online Coupling of Ion Exchange Resins." Analytical Chemistry **86**(10): 4668-4674.

Halliwell, B. and J. M. C. Gutteridge (1986). "Oxygen free radicals and iron in relation to biology and medicine: Some problems and concepts." Archives of Biochemistry and Biophysics **246**(2): 501-514.

Harris, E., B. Sinha, et al. (2012). "Sulfur isotope fractionation during heterogeneous oxidation of SO2 on mineral dust." Atmospheric Chemistry and Physics **12**(11): 4867-4884.

Harris, E., B. Sinha, et al. (2013). "Enhanced Role of Transition Metal Ion Catalysis During In-Cloud Oxidation of SO2." Science **340**(6133): 727-730.

Hinds, W. C. (1999). Aerosol technology : properties, behavior, and measurement of airborne particles. New York, Wiley.

Hineman, A. and C. Stephan (2014). "Effect of dwell time on single particle inductively coupled plasma mass spectrometry data acquisition quality." Journal of Analytical Atomic Spectrometry **29**(7): 1252-1257.

Hu, S., A. Polidori, et al. (2008). "Redox activity and chemical speciation of size fractioned PM in the communities of the Los Angeles-Long Beach harbor." Atmospheric Chemistry and Physics **8**(21): 6439-6451.

Ito, A. and L. Xu (2014). "Response of acid mobilization of iron-containing mineral dust to improvement of air quality projected in the future." Atmospheric Chemistry and Physics **14**(7): 3441-3459.

Jeong, G. Y. and E. P. Achterberg (2014). "Chemistry and mineralogy of clay minerals in Asian and Saharan dusts and the implications for iron supply to the oceans." Atmos Chem Phys **14**(22): 12415-12428.

Jickells, T. D., Z. S. An, et al. (2005). "Global iron connections between desert dust, ocean biogeochemistry, and climate." Science **308**(5718): 67-71.

Jickells, T. D. and L. J. Spokes (2001). "Atmospheric iron inputs to the oceans." IUPAC series on analytical and physical chemistry of environmental systems **7**: 85-122.

Johansen, A. M., R. L. Siefert, et al. (2000a). "Chemical composition of aerosols collected over the tropical North Atlantic Ocean." Journal of Geophysical Research: Atmospheres **105**(D12): 15277-15312.

Johansen, A. M., R. L. Siefert, et al. (2000b). "Chemical composition of aerosols collected over the tropical North Atlantic Ocean." Journal of Geophysical Research-Atmospheres **105**(D12): 15277-15312.

Johansson, C. and P. A. Johansson (2003). "Particulate matter in the underground of Stockholm." Atmospheric Environment **37**(1): 3-9.

Journet, E., K. V. Desboeufs, et al. (2008). "Mineralogy as a critical factor of dust iron solubility." Geophysical Research Letters **35**(7).

Kallos, G., M. Astitha, et al. (2007). "Long-range transport of anthropogenically and naturally produced particulate matter in the Mediterranean and North Atlantic: Current state of knowledge." Journal of Applied Meteorology and Climatology **46**(8): 1230-1251.

Kam, W., K. Cheung, et al. (2011a). "Particulate matter (PM) concentrations in underground and ground-level rail systems of the Los Angeles Metro." Atmospheric Environment **45**(8): 1506-1516.

Kam, W., R. J. Delfino, et al. (2013). "A comparative assessment of PM2.5 exposures in light-rail, subway, freeway, and surface street environments in Los Angeles and estimated lung cancer risk." Environmental Science-Processes & Impacts **15**(1): 234-243.

Kam, W., Z. Ning, et al. (2011b). "Chemical Characterization and Redox Potential of Coarse and Fine Particulate Matter (PM) in Underground and Ground-Level Rail Systems of the Los Angeles Metro." Environmental Science & Technology **45**(16): 6769-6776.

Karlsson, H. L., L. Nilsson, et al. (2005). "Subway particles are more genotoxic than street particles and induce oxidative stress in cultured human lung cells." Chemical Research in Toxicology **18**(1): 19-23.

Kim, J. B., S. Kim, et al. (2014). "Status of PM in Seoul metropolitan subway cabins and effectiveness of subway cabin air purifier (SCAP)." Clean Technologies and Environmental Policy **16**(6): 1193-1200.

Kim, K. Y., Y. S. Kim, et al. (2008). "Spatial distribution of particulate matter (PM10 and PM2.5) in Seoul Metropolitan Subway stations." Journal of Hazardous Materials **154**(1–3): 440-443.

Kong, L. D., X. Zhao, et al. (2014). "The effects of nitrate on the heterogeneous uptake of sulfur dioxide on hematite." Atmospheric Chemistry and Physics **14**(17): 9451-9467.

Laborda, F., E. Bolea, et al. (2014). "Single Particle Inductively Coupled Plasma Mass Spectrometry: A Powerful Tool for Nanoanalysis." Analytical Chemistry **86**(5): 2270-2278.

Landreman, A. P., M. M. Shafer, et al. (2008). "A macrophage-based method for the assessment of the reactive oxygen species (ROS) activity of atmospheric particulate matter (PM) and application to routine (daily-24 h) aerosol monitoring studies." Aerosol Science and Technology **42**(11): 946-957.

Leitch, M. E., E. Casman, et al. (2012). "Nanotechnology patenting trends through an environmental lens: analysis of materials and applications." Journal of Nanoparticle Research **14**(12).

Lighty, J. S., J. M. Veranth, et al. (2000). "Combustion aerosols: Factors governing their size and composition and implications to human health." Journal of the Air & Waste Management Association **50**(9): 1565-1618.

Liu, J., K. E. Murphy, et al. (2014). "Capabilities of Single Particle Inductively Coupled Plasma Mass Spectrometry for the Size Measurement of Nanoparticles: A Case Study on Gold Nanoparticles." Analytical Chemistry **86**(7): 3405-3414.

Lough, G. C., J. J. Schauer, et al. (2005). "Emissions of Metals Associated with Motor Vehicle Roadways." Environmental Science & Technology **39**(3): 826-836.

Luo, C., N. Mahowald, et al. (2008). "Combustion iron distribution and deposition." Global Biogeochemical Cycles **22**(1).

Luo, C., N. M. Mahowald, et al. (2005). "Estimation of iron solubility from observations and a global aerosol model." Journal of Geophysical Research-Atmospheres **110**(D23).

MacDonald, R. W., L. A. Barrie, et al. (2000). "Contaminants in the Canadian Arctic: 5 years of progress in understanding sources, occurrence and pathways." Science of the Total Environment **254**(2-3): 93-234.

Macdonald, R. W., T. Harner, et al. (2005). "Recent climate change in the Arctic and its impact on contaminant pathways and interpretation of temporal trend data." Science of the Total Environment **342**(1-3): 5-86.

Mahowald, N. M., A. R. Baker, et al. (2005). "Atmospheric global dust cycle and iron inputs to the ocean." Global Biogeochemical Cycles **19**(4).

Mahowald, N. M., S. Engelstaedter, et al. (2009). "Atmospheric Iron Deposition: Global Distribution, Variability, and Human Perturbations." Annual Review of Marine Science **1**: 245-278.

Majestic, B. J., A. D. Anbar, et al. (2009a). "Elemental and iron isotopic composition of aerosols collected in a parking structure." Science of the Total Environment **407**(18): 5104-5109.

Majestic, B. J., A. D. Anbar, et al. (2009b). "Stable Isotopes as a Tool to Apportion Atmospheric Iron." Environmental Science & Technology **43**(12): 4327-4333.

Majestic, B. J., J. J. Schauer, et al. (2007a). "Application of synchrotron radiation for measurement of iron red-ox speciation in atmospherically processed aerosols." Atmospheric Chemistry and Physics **7**(10): 2475-2487.

Majestic, B. J., J. J. Schauer, et al. (2007b). "Development of a manganese speciation method for atmospheric aerosols in biologically and environmentally relevant fluids." Aerosol Science and Technology **41**(10): 925-933.

Majestic, B. J., J. J. Schauer, et al. (2008). "Trace metal analysis of atmospheric particulate matter: A comparison of personal and ambient samplers." Journal of Environmental Engineering and Science **7**(4): 289-298.

Majestic, B. J., J. J. Schauer, et al. (2006). "Development of a Wet-Chemical Method for the Speciation of Iron in Atmospheric Aerosols." Environmental Science & Technology **40**(7): 2346-2351.

Manoli, E., D. Voutsa, et al. (2002). "Chemical characterization and source identification/apportionment of fine and coarse air particles in Thessaloniki, Greece." Atmospheric Environment **36**(6): 949-961.

Mason, R. P. (2013). Trace metals in aquatic systems.

McCurdy, E. and D. Potter (2001). "Optimising ICP/MS for the determination of trace metals in high matrix samples." Spectroscopy Europe **13**(3): 14-21.

Mead, C., P. Herckes, et al. (2013). "Source apportionment of aerosol iron in the marine environment using iron isotope analysis." Geophysical Research Letters **40**(21): 5722-5727.

Meskhidze, N., W. L. Chameides, et al. (2003). "Iron mobilization in mineral dust: Can anthropogenic SO2 emissions affect ocean productivity?" Geophysical Research Letters **30**(21).

Misra, C., M. Singh, et al. (2002). "Development and evaluation of a personal cascade impactor sampler (PCIS)." Journal of Aerosol Science **33**(7): 1027-1047.

Mitrano, D. M., E. K. Lesher, et al. (2012). "Detecting nanoparticulate silver using single-particle inductively coupled plasma–mass spectrometry." Environmental Toxicology and Chemistry **31**(1): 115-121.

Montano, M. D., H. R. Badiei, et al. (2014). "Improvements in the detection and characterization of engineered nanoparticles using spICP-MS with microsecond dwell times." Environmental Science-Nano **1**(4): 338-346.

Montoya, L. D. and L. M. Hildemann (2005). "Size distributions and height variations of airborne particulate matter and cat allergen indoors immediately following dust-disturbing activities." Journal of Aerosol Science **36**(5-6): 735-749.

Moore, J. K., S. C. Doney, et al. (2002). "Iron cycling and nutrient-limitation patterns in surface waters of the World Ocean." Deep-Sea Research Part Ii-Topical Studies in Oceanography **49**(1-3): 463-507.

Mortimer, K. M., L. M. Neas, et al. (2002). "The effect of air pollution on inner-city children with asthma." European Respiratory Journal **19**(4): 699-705.

Mugica-Alvarez, V., J. Figueroa-Lara, et al. (2012). "Concentrations and properties of airborne particles in the Mexico City subway system." Atmospheric Environment **49**: 284-293.

Murruni, L. G., V. Solanes, et al. (2009). "Concentrations and elemental composition of particulate matter in the Buenos Aires underground system." Atmospheric Environment **43**(30): 4577-4583.

Nico, P. S., B. M. Kumfer, et al. (2009). "Redox Dynamics of Mixed Metal (Mn, Cr, and Fe) Ultrafine Particles." Aerosol Science and Technology **43**(1): 60-70.

Oakes, M., E. D. Ingall, et al. (2012a). "Iron Solubility Related to Particle Sulfur Content in Source Emission and Ambient Fine Particles." Environmental Science & Technology **46**(12): 6637-6644.

Oakes, M., R. J. Weber, et al. (2012b). "Characterization of iron speciation in urban and rural single particles using XANES spectroscopy and micro X-ray fluorescence measurements: investigating the relationship between speciation and fractional iron solubility." Atmospheric Chemistry and Physics **12**(2): 745-756.

Ooki, A., J. Nishioka, et al. (2009). "Size dependence of iron solubility of Asian mineral dust particles." Journal of Geophysical Research: Atmospheres **114**(D3): D03202.

Pace, H. E., N. J. Rogers, et al. (2012). "Single Particle Inductively Coupled Plasma-Mass Spectrometry: A Performance Evaluation and Method Comparison in the Determination of Nanoparticle Size." Environmental Science & Technology **46**(22): 12272-12280.

Pace, H. E., N. J. Rogers, et al. (2011). "Determining Transport Efficiency for the Purpose of Counting and Sizing Nanoparticles via Single Particle Inductively Coupled Plasma Mass Spectrometry." Analytical Chemistry **83**(24): 9361-9369.

Paris, R. and K. V. Desboeufs (2013). "Effect of atmospheric organic complexation on iron-bearing dust solubility." Atmospheric Chemistry and Physics **13**(9): 4895-4905.

Paris, R., K. V. Desboeufs, et al. (2010). "Chemical characterisation of iron in dust and biomass burning aerosols during AMMA-SOP0/DABEX: implication for iron solubility." Atmospheric Chemistry and Physics **10**(9): 4273-4282.

Pilinis, C., J. H. Seinfeld, et al. (1989). "Water content of atmospheric aerosols." Atmospheric Environment **23**(7): 1601-1606.

Pope, C. A. and D. W. Dockery (2006). "Health Effects of Fine Particulate Air Pollution: Lines that Connect." Journal of the Air & Waste Management Association **56**(6): 709-742.

Prophete, C., P. Maciejczyk, et al. (2006). "Effects of select PM-associated metals on alveolar macrophage phosphorylated ERK1 and-2 and iNOS expression during ongoing alteration in iron homeostasis." Journal of Toxicology and Environmental Health, Part A: Current Issues **69**(10): 935-951.

Prospero, J. M., P. Ginoux, et al. (2002). "Environmental characterization of global sources of atmospheric soil dust identified with the Nimbus 7 Total Ozone Mapping Spectrometer (TOMS) absorbing aerosol product." Reviews of Geophysics **40**(1).

Querol, X., T. Moreno, et al. (2012). "Variability of levels and composition of PM10 and PM2.5 in the Barcelona metro system." Atmospheric Chemistry and Physics **12**(11): 5055-5076.

Querol, X., M. Viana, et al. (2007). "Source origin of trace elements in PM from regional background, urban and industrial sites of Spain." Atmospheric Environment **41**(34): 7219-7231.

Raut, J. C., P. Chazette, et al. (2009). "Link between aerosol optical, microphysical and chemical measurements in an underground railway station in Paris." Atmospheric Environment **43**(4): 860-868.

Rosati, J. A., J. Thornburg, et al. (2008). "Resuspension of particulate matter from carpet due to human activity." Aerosol Science and Technology **42**(6): 472-482.

Rubin, A. J. (1974). Aqueous-environmental chemistry of metals. Ann Arbor, Mich., Ann Arbor Science Publishers.

Saffari, A., N. Daher, et al. (2013). "Seasonal and spatial variation of trace elements and metals in quasi-ultrafine (PM0.25) particles in the Los Angeles metropolitan area and characterization of their sources." Environmental Pollution **181**: 14-23.

Salma, I., M. Posfai, et al. (2009). "Properties and sources of individual particles and some chemical species in the aerosol of a metropolitan underground railway station." Atmospheric Environment **43**(22-23): 3460-3466.

Salma, I., T. Weidinger, et al. (2007). "Time-resolved mass concentration, composition and sources of aerosol particles in a metropolitan underground railway station." Atmospheric Environment **41**(37): 8391-8405.

Sammut, M. L., Y. Noack, et al. (2010). "Speciation of Cd and Pb in dust emitted from sinter plant." Chemosphere **78**(4): 445-450.

Sammut, M. L., J. Rose, et al. (2008). "Determination of zinc speciation in basic oxygen furnace flying dust by chemical extractions and X-ray spectroscopy." Chemosphere **70**(11): 1945-1951.

Seaton, A., J. Cherrie, et al. (2005). "The London Underground: dust and hazards to health." Occupational and Environmental Medicine **62**(6): 355-362.

Seinfeld, J. H. and S. N. Pandis (2006). Atmospheric Chemistry and Physics: From Air Pollution to Climate Change, John Wiley & Sons.

Seo, J., D. Kwon, et al. (2010). "Potential Risks of the Natural Nanoparticles from the Acid Mine Drainage and a Novel Approach for Their Toxicity Assessment." Toxicology and Environmental Health Sciences **2**(4): 215-220.

Shafer, M. M., B. M. Toner, et al. (2012). "Chemical Speciation of Vanadium in Particulate Matter Emitted from Diesel Vehicles and Urban Atmospheric Aerosols." Environmental Science & Technology **46**(1): 189-195.

Sholkovitz, E. R., P. N. Sedwick, et al. (2009). "Influence of anthropogenic combustion emissions on the deposition of soluble aerosol iron to the ocean: Empirical estimates for island sites in the North Atlantic." Geochimica Et Cosmochimica Acta **73**(14): 3981-4003.

Sholkovitz, E. R., P. N. Sedwick, et al. (2012). "Fractional solubility of aerosol iron: Synthesis of a global-scale data set." Geochimica Et Cosmochimica Acta **89**: 173-189.

Siefert, R. L., S. M. Webb, et al. (1996). "Determination of photochemically available iron in ambient aerosols." Journal of Geophysical Research-Atmospheres **101**(D9): 14441-14449.

Singh, M., P. A. Jaques, et al. (2002). "Size distribution and diurnal characteristics of particle-bound metals in source and receptor sites of the Los Angeles Basin." Atmospheric Environment **36**(10): 1675-1689.

Singh, M., C. Misra, et al. (2003). "Field evaluation of a personal cascade impactor sampler (PCIS)." Atmospheric Environment **37**(34): 4781-4793.

Song, Y., D. D. Xu, et al. (2006). "INAA study for characterization of PM10 and PM2.5 in Beijing and influence of dust storm." Journal of Radioanalytical and Nuclear Chemistry **270**(1): 29-33.

Spokes, L. J., T. D. Jickells, et al. (1994). "Solubilization of aerosol trace-metals by cloud processing-a laboratory study." Geochimica Et Cosmochimica Acta **58**(15): 3281-3287.

Stookey, L. L. (1970). "Ferrozine - a New Spectrophotometric Reagent for Iron." Analytical Chemistry **42**(7): 779-&.

Strenge, I. and C. Engelhard (2015). "Capabilities of fast data acquisition with microsecond time resolution in inductively coupled plasma mass spectrometry and identification of signal artifacts from millisecond dwell times during detection of single gold nanoparticles." Journal of Analytical Atomic Spectrometry.

Stumm, W. and J. J. Morgan (1996). Aquatic Chemistry. New York, J. Wiley-Interscience.

Tao, F., B. Gonzalez-Flecha, et al. (2003). "Reactive oxygen species in pulmonary inflammation by ambient particulates." Free Radical Biology and Medicine **35**(4): 327-340.

Taylor, S. R. and S. M. Mclennan (1995). "The Geochemical Evolution of the Continental-Crust." Reviews of Geophysics **33**(2): 241-265.

Thurston, G. D. and J. D. Spengler (1985). "A quantitative assessment of source contributions to inhalable particulate matter pollution in metropolitan Boston." Atmospheric Environment (1967) **19**(1): 9-25.

Tiwari, G. N., H. N. Singh, et al. (2003). "Present status of solar distillation." Solar Energy **75**(5): 367-373.

Turner, A. and G. E. Millward (2002). "Suspended particles: Their role in estuarine biogeochemical cycles." Estuarine Coastal and Shelf Science **55**(6): 857-883.

Upadhyay, N., B. J. Majestic, et al. (2011). "Solubility and speciation of atmospheric iron in buffer systems simulating cloud conditions." Atmospheric Environment **45**(10): 1858-1866.

Valavanidis, A., K. Fiotakis, et al. (2005). "Electron paramagnetic resonance study of the generation of reactive oxygen species catalysed by transition metals and quinoid redox cycling by inhalable ambient particulate matter." Redox Report **10**(1): 37-51.

Verma, V., M. M. Shafer, et al. (2010). "Contribution of transition metals in the reactive oxygen species activity of PM emissions from retrofitted heavy-duty vehicles." Atmospheric Environment **44**(39): 5165-5173.

Veysseyre, A., K. Moutard, et al. (2001). "Heavy metals in fresh snow collected at different altitudes in the Chamonix and Maurienne valleys, French Alps: initial results." Atmospheric Environment **35**(2): 415-425.

von der Heyden, B. P., A. N. Roychoudhury, et al. (2012). "Chemically and Geographically Distinct Solid-Phase Iron Pools in the Southern Ocean." Science **338**(6111): 1199-1201.

Werner, M., P. Nico, et al. (2006). "Laboratory Study of Simulated Atmospheric Transformations of Chromium in Ultrafine Combustion Aerosol Particles." Aerosol Science and Technology **40**(7): 545-556.

Wu, J., E. Boyle, et al. (2001). "Soluble and Colloidal Iron in the Oligotrophic North Atlantic and North Pacific." Science **293**(5531): 847-849.

Wu, J., R. Rember, et al. (2007). "Dissolution of aerosol iron in the surface waters of the North Pacific and North Atlantic oceans as determined by a semicontinuous flow-through reactor method." Global Biogeochemical Cycles **21**(4): GB4010.

Zhang, J. (1995). "Geochemistry of Trace Metals from Chinese River/Estuary Systems: An Overview." Estuarine Coastal and Shelf Science **41**(6): 631-658.

Zhuang, G. S., Z. Yi, et al. (1992). "Link between Iron and Sulfur Cycles Suggested by Detection of Fe(II) in Remote Marine Aerosols." Nature **355**(6360): 537-539.

Appendix A

Figure with axis labels: Y-axis "CDPHE TEOM Data (μg m^{-3})", X-axis "CAMP DU Data (μg m^{-3})". Equation shown: $y = 1.1092x + 0.1271$, $R^2 = 0.9999$.
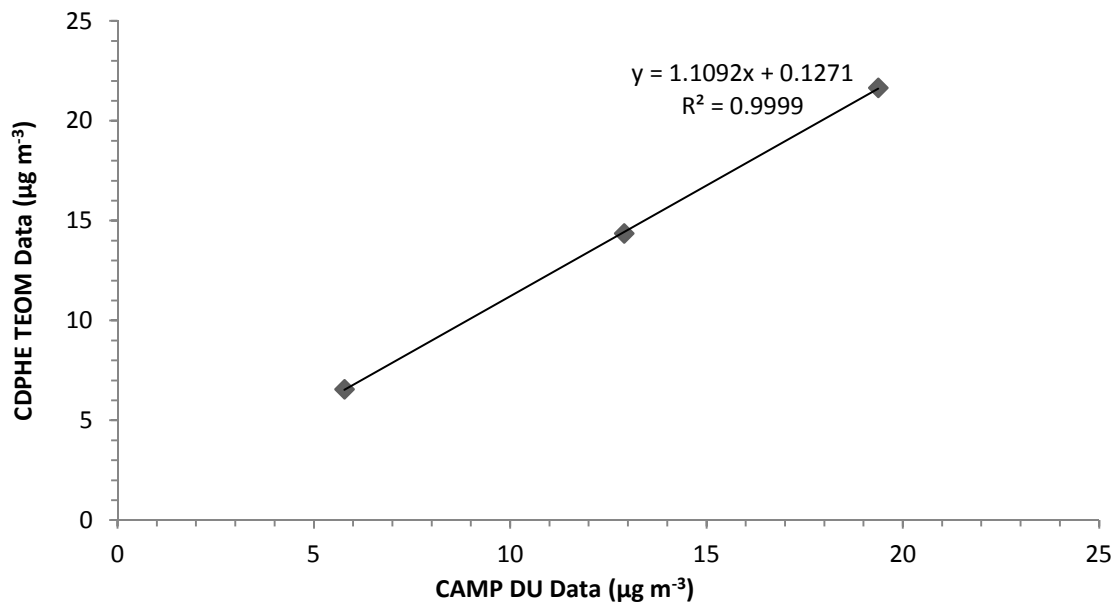
Figure A1: PM$_{2.5}$ correlation plot between real-time PM$_{2.5}$ concentration measurements by the Colorado Department of Public Health and Environment (CDPHE) and calculated PM$_{2.5}$ concentrations made from this study (CAMP DU Data). Plotted values are PM$_{2.5}$ concentrations of each sample collection period.

Table A1: Geometric mean and standard deviation (dimensionless) of PM$_{2.5}$ size fractions.

Site:	Downtown	Track-side	On board
Size Fraction (µm)			
2.5-1.0	1.2 ± 1.0	1.2 ± 1.0	1.1 ± 1.1
1.0-0.5	1.0 ± 1.0	0.9 ± 1.0	1.0 ± 1.0
0.5-0.25	0.5 ± 1.1	0.3 ± 1.0	0.7 ± 1.4
0.25-0.02*	0.01 ± 300	0.02 ± 14	0.2 ± 5.0

*Large standard deviation due to the lower size limit (0.02 µm) being assumed.

Appendix B

Table B1: Statistical results of T-tests comparing particle size fractions. Size fractions compared for each test are shown in the size column headers.

Mineral	Condition	Size Fraction (µm)					
		10-2.5 vs 2.5-1.0	10-2.5 vs 1.0-0.5	10-2.5 vs 0.5-0.25	2.5-1.0 vs 1.0-0.5	2.5-1.0 vs 0.5-0.25	1.0-0.5 vs 0.5-0.25
Goethite	High RH + SO$_2$	0.50	0.33	0.11	0.29	0.09	0.003*
Goethite	Low RH + SO$_2$	0.03*	0.11	0.01*	0.18	0.004*	0.07
Goethite	High RH + No SO$_2$	0.03*	0.33	0.19	0.22	0.18	0.24
Goethite	Low RH + No SO$_2$	0.43	0.49	0.12	0.30	0.17	0.16
Magnetite	High RH + SO$_2$	0.20	0.15	0.18	0.02*	0.40	0.47
Magnetite	Low RH + SO$_2$	0.20	0.17	0.07	0.05	0.36	0.43
Magnetite	High RH + No SO$_2$	0.15	0.18	0.02*	0.19	0.46	0.26
Magnetite	Low RH + No SO$_2$	0.15	0.14	0.16	0.15	0.22	0.37
Hematite	High RH + SO$_2$	0.33	0.07	0.001*	0.01*	0.001*	0.001*
Hematite	Low RH + SO$_2$	0.15	0.05*	0.20	0.35	0.22	0.21
Hematite	High RH + No SO$_2$	0.35	0.01*	0.08	0.03*	0.08	0.09
Hematite	Low RH + No SO$_2$	0.29	0.21	0.19	0.21	0.19	0.21

Table B2: Statistical results of T-tests comparing the effects of relative humidity (high RH vs low RH).

Mineral	Size Fraction (μm)	SO_2 High RH vs Low RH	No SO_2 High RH vs Low RH
		Experimental Conditions	
Goethite	10-2.5	0.09	0.08
Goethite	2.5-1.0	0.02*	0.10
Goethite	1.0-0.5	0.19	0.21
Goethite	0.5-0.25	0.37	0.48
Magnetite	10-2.5	0.24	0.29
Magnetite	2.5-1.0	0.20	0.14
Magnetite	1.0-0.5	0.15	0.19
Magnetite	0.5-0.25	0.38	0.26
Hematite	10-2.5	0.17	0.14
Hematite	2.5-1.0	0.12	0.19
Hematite	1.0-0.5	0.10	0.21
Hematite	0.5-0.25	0.23	0.22

* represents statistical difference ($p < 0.05$).

Table B3: Statistical results of T-tests comparing the effects of sulfur dioxide exposure (SO_2 vs No SO_2).

Mineral	Size Fraction (µm)	Experimental Conditions	
		High RH SO_2 vs No SO_2	Low RH SO_2 vs No SO_2
Goethite	10-2.5	0.18	0.38
Goethite	2.5-1.0	0.24	0.07
Goethite	1.0-0.5	0.39	0.15
Goethite	0.5-0.25	0.40	0.35
Magnetite	10-2.5	0.27	0.08
Magnetite	2.5-1.0	0.26	0.20
Magnetite	1.0-0.5	0.21	0.24
Magnetite	0.5-0.25	0.30	0.24
Hematite	10-2.5	0.18	0.17
Hematite	2.5-1.0	0.19	0.28
Hematite	1.0-0.5	0.20	0.21
Hematite	0.5-0.25	0.34	0.22

* represents statistical difference ($p < 0.05$)